The Meteoritical Society

Meteoritics & Planetary Science 1–29 (2024)
doi: 10.1111/maps.14251

Atmospheric collection of extraterrestrial dust at the Earth's surface in the mid-Pacific

Penelope J. WOZNIAKIEWICZ[1,2]*, Luke S. ALESBROOK[1], John P. BRADLEY[3], Hope A. ISHII[3], Mark C. PRICE[1,4], Michael. E. ZOLENSKY[5], Donald E. BROWNLEE[6], Matthias van GINNEKEN[1], and Matthew J. GENGE[2,7]

[1]Physics and Astronomy, University of Kent, Canterbury, Kent, UK
[2]Earth Sciences Department, Natural History Museum, London, UK
[3]Hawai'i Institute of Geophysics and Planetology, University of Hawai'i, Honolulu, Hawaii, USA
[4]ODIN Space Ltd, London, UK
[5]NASA Johnson Space Center (JSC), Houston, Texas, USA
[6]Department of Astronomy, University of Washington, Seattle, Washington, USA
[7]Department of Earth Science and Engineering, Imperial College London, London, UK

*Correspondence
Penelope J. Wozniakiewicz, Physics and Astronomy, University of Kent, Canterbury, Kent CT2 7NH, UK.
Email: pjw@kent.ac.uk

(*Received 15 July 2023; revision accepted 19 July 2024*)

Abstract–The Kwajalein micrometeorite collection utilized high volume air samplers fitted with polycarbonate membrane filters to capture particles directly from the atmosphere at the Earth's surface. This initial study focused on identifying cosmic spherule-like particles, conservatively categorizing them into four groups based on bulk compositional data: Group I exhibit a range of compositions designated terrestrial in origin; group II are Fe-rich and contain only additional O, S, and/or Ni; group III are silicate spherules with Mg-to-Si At% ratios less than 0.4; group IV are silicate spherules with Mg-to-Si At% ratios greater than 0.4. Spherules in groups I, II, and III have compositions that are also consistent with particles that are produced in great numbers by natural and/or anthropogenic terrestrial activities (e.g., volcanic microspherules, fly ash from coal fired power plants, etc.) and thus are assumed terrestrial in origin. Group IV spherules exhibit compositions closest to those of cosmic spherules identified in other collections and are, therefore, designated cosmic spherule candidates. Detailed analysis of seven group IV spherules found that whilst five exhibited morphology and compositions consistent with S-type cosmic spherules, two appear unique to this collection and could not be matched to either terrestrial or extraterrestrial spherules studied to date.

INTRODUCTION

Despite their small size, approximately (40 ± 20) × 10^6 kg yr^{-1} of extraterrestrial material arrives at the Earth in the form of dust (Love & Brownlee, 1993), greatly outweighing the estimated 5.38 × 10^4 kg yr^{-1} that arrives as larger meteorites (Zolensky et al., 2006). Much of this material is believed to burn up on atmospheric entry, yet it is estimated that ~15% does survive to arrive at the Earth's surface as micrometeorites (Rojas et al., 2021). Laboratory studies of micrometeorites to date suggest that, as with meteorites, most originate from asteroids and, in some cases, comets, the small bodies of our solar system—although this is contrary to the models of Nesvorný et al. (2010) and Carrillo-Sánchez et al. (2016) which predict most of the dust arriving at Earth (~85% or ~80% of the total mass flux, respectively) should be cometary in origin. Comets and asteroids are believed to contain

primordial solar system materials in various states of preservation, from unprocessed particles that have remained pristine since accretion, through to heavily altered or completely reprocessed materials that have experienced aqueous and thermal alteration on the parent body. The mineralogy of these materials can provide a record of the environments in which they formed (e.g., temperatures, materials available, and heating and cooling rates) and/or any subsequent processing they have experienced since accretion on their parent bodies (e.g., impacts, aqueous alteration). Compositional (major, minor, and trace element abundances), isotopic, and textural studies suggest that a large number of these micrometeorites share affinities with meteorite groups (Genge, 2008; Genge et al., 1997; Kurat et al., 1994; van Ginneken et al., 2017). Some, however, exhibit distinct characteristics attributed to bodies not represented in current meteorite collections, for example, ultracarbonaceous micrometeorites (Duprat et al., 2010; Nakamura et al., 2005) and chondritic porous micrometeorites (Noguchi et al., 2015). The presence of these more exotic materials amongst micrometeorites (and not meteorites) is perhaps a consequence of selection effects associated with atmospheric entry. For example, the gentler deceleration experienced by dust-sized grains while still in the upper atmosphere may be more conducive to fragile materials reaching the Earth's surface. Alternatively, it may represent an inherent difference between the sources of dust and larger rocky objects, with perhaps different size populations released by different processes acting/occurring on the parent body (e.g., impacts, natural fragmentation, and release of rocky materials through loss of binding volatiles, etc.) or differences in the make-up of the parent body and thus its material strength and fragmentation behavior when subject to, for example, impacts (e.g., as demonstrated by Flynn et al., 2009). Micrometeorites, therefore, complement, and expand upon, existing meteorite collections and could provide a more complete picture of the content and evolution of the solar system.

Compared to larger meteorites, micrometeorites have received far less attention in the literature to date. This is largely due to their diminutive size, which has required relatively recent technological advances to enable detailed analyses of such microgram to nanogram-sized samples (see Zolensky et al., 2000), but also due to difficulties in their collection. When micrometeorites are directly compared against natural and man-made terrestrial dust particles, they may be distinguished by the presence of a magnetite shell (if partially melted, with this feature the result of moderate atmospheric entry heating), Ni-bearing iron metal or chondritic bulk compositions as well as characteristic isotope and noble gas abundances (Genge et al., 2008). Micrometeorites may also exhibit further evidence of heating, such as sub-spherical particle morphologies resulting from partial or total melting. In addition, their olivines are commonly Fe-poor and contain Ca and Cr, which is rare amongst terrestrial rocks (Brearley & Jones, 1998). However, in most locations, background terrestrial dust vastly outnumbers the incoming micrometeorites, completely obscuring them and making the implementation of any grain-by-grain search and analysis an impossible feat. Consequently, the successful collection of micrometeorites requires either the application of some separation technique, or some approach whereby the amount of background terrestrial dust is limited. Below, we present different methods but for a recent summary of individual collections, including strengths, weaknesses, and biases of each, we direct the reader to van Ginneken et al. (2024).

A common separation technique has been the use of magnets to isolate metal and magnetite-bearing micrometeorites. This has been successfully applied to separate micrometeorites from deep-sea sediments (e.g., Brownlee et al., 1979; Fredriksson, 1956; Pettersson & Fredriksson, 1958) and dissolved pre-historic limestones (e.g., Dredge et al., 2010), chalk (e.g., Suttle & Genge, 2017) and salts (e.g., Davidson et al., 2007). Such separation methods have even been able to identify micrometeorites in accumulated sediments taken from rooftops in urban areas (e.g., Genge et al., 2017; Jonker et al., 2023; Larsen, 2016; Suttle et al., 2021). In the cases of those removed from rocks, samples are further complicated by geological processing. Those so far collected from urban rooftops exhibit varying degrees of weathering via exposure to Earth's environment, with spherules ranging from minimally to severely altered (e.g., Jonker et al., 2023; Suttle et al., 2021). However, for all of these collections that utilize magnetic separation to narrow down their searches, the resulting samples do not represent the entire incident population of micrometeorites.

To instead limit the background terrestrial dust, we may seek to perform collections in remote locations where the terrestrial dust flux is much lower, and micrometeorites represent a larger fraction of the incoming dust component. For example, micrometeorites have been successfully extracted from glacial sediments in the Antarctic (e.g., Genge et al., 2018; Goderis et al., 2020; Rochette et al., 2008). These studies suggest that the sampled sediments have been accumulating for 1 Myr or more. As a consequence, they contain some of the largest examples of micrometeorites identified to date (e.g., Rochette et al., 2008; Suavet et al., 2009, 2011; van Ginneken et al., 2012). However, such long duration of exposure to the terrestrial environment also means that these samples exhibit evidence of considerable weathering that hinders attempts to characterize and classify particles, and investigate the effects of atmospheric entry

alteration (see, e.g., van Ginneken et al., 2016). Since terrestrial sediments still vastly outnumber the extraterrestrial particles contained in these glacial sediments, most studies have also opted to use magnetic separation to further concentrate the micrometeorites prior to search and extraction.

Micrometeorite collections have also been successfully obtained from Antarctic ice and snow without the need for magnetic separation (e.g., Duprat et al., 2007; Engrand & Maurette, 1998; Maurette et al., 1991; Noguchi et al., 2000; Taylor et al., 1998). Those extracted from ice are several hundreds to thousands of years old and consequently, these samples also exhibit varying degrees of weathering (e.g., Suzuki et al., 2010; Terada et al., 2001). In contrast, samples extracted from snow have arrival times of a couple of years to decades prior to collection and appear minimally altered (e.g., Duprat et al., 2007; Noguchi et al., 2015). These snow samples are proving to be invaluable to the understanding of interplanetary dust, and the parent bodies from which they are derived. Further efforts to continue characterizing these collections together with the development of more effective methods of collection for the new material will, no doubt, lead to more discoveries.

In the last decade, other attempts have been made to perform collections beyond these cold desert environments, with micrometeorite samples returned from surface sands of hot deserts, such as the Atacama (e.g., van Ginneken et al., 2017). There, as with glacial sediment collections, the low sedimentation rate of terrestrial dust means that the surface sands have been accumulating for a long period of time, maximizing micrometeorite numbers in any sample taken. However, also similar to glacial sediments, terrestrial alteration is observed in these samples.

An alternative approach to limit the background terrestrial dust is to sample directly from the atmosphere. Several atmospheric collection methods have been developed to perform collections in the stratosphere where terrestrial contamination is significantly reduced. Initially using balloon-borne collectors (e.g., the "Vacuum monster;" Brownlee et al., 1973) and later using collectors attached to NASA high-altitude aircraft (e.g., U2 aircraft; Brownlee, 1977), extraterrestrial dust particles have been collected from the stratosphere for almost 50 years. These collectors capture particles, referred to as interplanetary dust particles (IDPs), by inertial impaction, a process whereby the air (containing particles) moves past the collector surface at sufficiently high velocity that micron-sized particles impact the collector while air molecules and the smaller particles pass around it. As collection times and dates can be scheduled for each flight, sampling can be performed to coincide with known celestial events such as meteor showers (Messenger, 2002); therefore, unlike for particles from surface collections detailed previously, we may potentially be able to link individual samples to specific parent bodies. For example, attempts to perform such targeted IDP collections include the November 2002 flights to coincide with Leonid storm debris from comet 55P/Tempel-Tuttle (Rietmeijer et al., 2003) and the April 2003 flights to coincide with the Earth crossing stream of particles from comet Grigg-Skjellerup (https://www-curator.jsc.nasa.gov/dust/leonid_shwr_grigg_skjellerup.cfm). This is a vast improvement on the surface collections detailed earlier, where knowledge of an individual particle's arrival time can be stated to, at best, ±years or ± decades. In both balloon and aircraft-based collectors, however, capture of the particles has been achieved by coating collection surfaces in sticky silicone oil. The use of silicone oil, whilst an efficient capture medium, is problematic; despite efforts to remove silicone oil using organic solvents (typically hexane) samples are often found to exhibit silicone oil contamination (e.g., Bradley et al., 2014; Schramm et al., 1989). In addition, there is concern that such harsh washing methods may remove any indigenous soluble organics. This has prompted the dust collection community to investigate alternative methods for atmospheric collections such as stratospheric flights employing collectors composed of polyurethane foam (Messenger et al., 2015).

In this paper, we describe our efforts in 2011/2012 to test a micrometeorite collection method that utilizes high-volume air samplers to filter particles directly from the atmosphere at the Earth's surface. By collecting directly from the atmosphere, particles are collected before they can land and become lost amongst the vast quantities of terrestrial dust. Our ground-based atmospheric collection method also avoids the use of silicone oil and associated harsh washing techniques by employing polycarbonate membrane filters with 5-μm-diameter laser-etched perforations, to which the particles adhere via van der Waals forces. Being ground based, it also avoids the need for access to high-altitude aircraft/balloons, making its use potentially possible in any location with access to a power supply. Compared to other ground-based techniques, particle arrival times for our collections can be better constrained: Using the falling speeds calculated by Karsten (1968) for a 20-μm spherical grain of density 1 g cm^{-3} descending from an altitude of 80 km, the time taken to settle to the Earth's surface is estimated to be on the order of 26 days. While this is grossly simplified, not taking into account any physical properties of the particle and assuming direct descent to the surface with no influence from, for example, atmospheric circulation, this suggests that arrival times for any particle on a filter can be estimated within ±weeks to months and, as with stratospheric collections, potential links with meteor showers may be possible. In designing this collection, it was also hoped

that the short collection periods combined with collection directly from the air (such that they are not contained within snow/water/ice) would mean that the terrestrial age of, and weathering (both chemical and mechanical) experienced by, the particles would be minimized. As a consequence, it was hoped that perhaps our collections may include particles that are either not well preserved or are absent in other ground-based collections.

Our collection site, the mid-Pacific, aimed to test this collection method in locations other than the traditional cold desert settings of previous collections. A similar ground-based atmospheric collection has since been set up in the Antarctic and has already reported promising initial results (Taylor et al., 2020).

METHOD

The tests of our ground-based atmospheric collection method were performed in 2011/2012 on Kwajalein Island in the Republic of the Marshall Islands in the Pacific Ocean (Wozniakiewicz et al., 2011, 2014). Collecting at this location exploits the considerably reduced anthropogenic background; Kwajalein is >1000 miles from the nearest continent and for much of the year, trade winds blow from the northeast at 15–20 knots providing a continuous stream of ocean air from which to sample.

Two high-volume air samplers (HVP 4000 series with automatic flow control from Hi-Q Environmental) were installed on top of the two-story airport building on Kwajalein, upwind of local anthropogenic sources of aerosols (Figure 1a). Although not as busy as other airports, we still recognize the potential for contributions from aircraft to the filters; however, the selection of this location was necessitated by the requirement for a platform located at least one story up (to minimize surface dust contributions via saltation), which was both easily accessible and had a power source within reach. These samplers monitored and adjusted the flow rate to that set, and continuously provided a readout of the initially set and current flow rate, the time elapsed and the current total volume of air filtered. Upon each filter exchange, the total volume of air filtered was noted down, and the sampler was reset. The samplers were fitted with polycarbonate membrane filters (Figure 1b) with 5-μm-diameter laser-etched perforations. Initial tests during setup on Kwajalein found that the sampler motors were put under significant strain and overheated after a day in this environment when run at their highest flow rate (~1 m^3 per minute). An initial flow rate of 0.5 m^3 per minute was, therefore, adopted, with filters being changed weekly. Prior to exposure, these filters were mounted between two thin acrylic frames to facilitate handling, and additional acrylic sheets and a spacer frame were utilized to encase framed filters and prevent damage and contamination during storage and transportation before and after exposure (Figure 2). All filter preparation was performed in a clean room. The samplers were run continuously from mid-October 2011 to early January 2012 and again from mid-May 2012 to late August 2012. A power surge in early January 2012 damaged internal components of both samplers, resulting in their being out of action between January and May of that year while replacement parts were being ordered, shipped, and

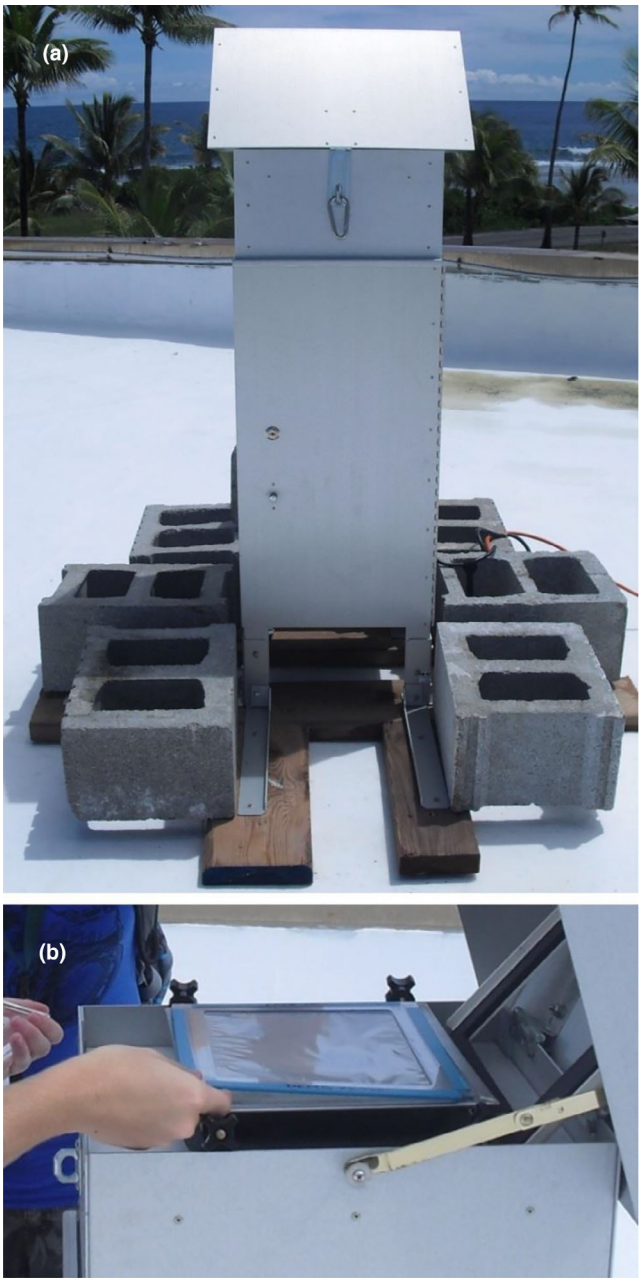

Figure 1. Photo of: (a) One of the high-volume air samplers located on the airport building on Kwajalein. (b) Filter change being performed.

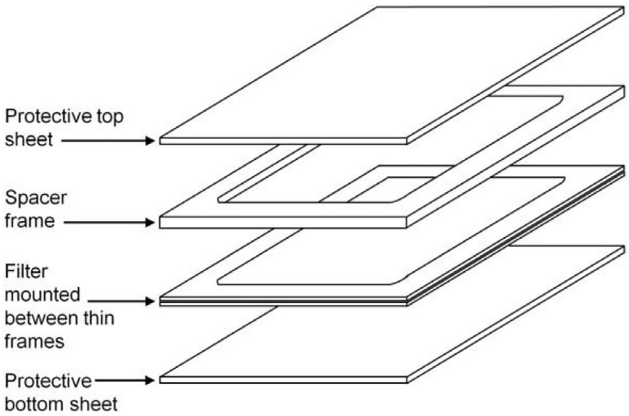

Figure 2. Schematic of acrylic sheets and frames used to provide a protective casing for filters during storage/transportation. An additional thick spacer frame ensures the filter collection surface does not touch the protective acrylic top sheet. The entire assembly was held together during storage/transportation by four large metal bulldog clips. Filter collection areas measure ~203 mm × 254 mm.

fitted. Once complete, the filters were shipped to the UK for study.

Due to the humid, salt-laden environment of Kwajalein, all of the filters appeared to be wet when they arrived in the UK. Assuming this liquid had been present since sampling occurred, the particles could have been in damp conditions for up to 18 months (with the longest exposure for those filters collected earliest). On arrival, filters were sealed in a laminar flow cabinet with desiccator cartridges and the airflow was turned off. On drying out all of the filters developed a coating of salt. In order to study the samples, a method of removing the salt was needed. The filters are also very large, measuring ~203 × 254 mm (Figure 2), an area over which it would be impractical to search for all micrometeorite candidates. It was, therefore, also necessary to devise a method of concentrating the particles in a smaller area on the filters prior to searching for micrometeorites. To satisfy both of these needs, high-purity water was used to dissolve the salt and dislodge the particles, while simultaneously using a small vacuum pump beneath to create a well at the center of the filter to concentrate the particles here and remove the salt water (Figure 3a,b). After washing and concentration, the central areas of the filters were mounted on conductive carbon adhesive on large (50 mm) Al stubs, cut free, and allowed to dry naturally in a sealed laminar flow cabinet (flow turned off and containing several desiccator cartridges) ready for analysis (Figures 3c and 4).

Tests were performed using this washing method on filters which had been loaded with 100-μm glass spheres and fluffy aggregate grains (chondritic porous IDP analogs used and described in Kearsley et al., 2009 and

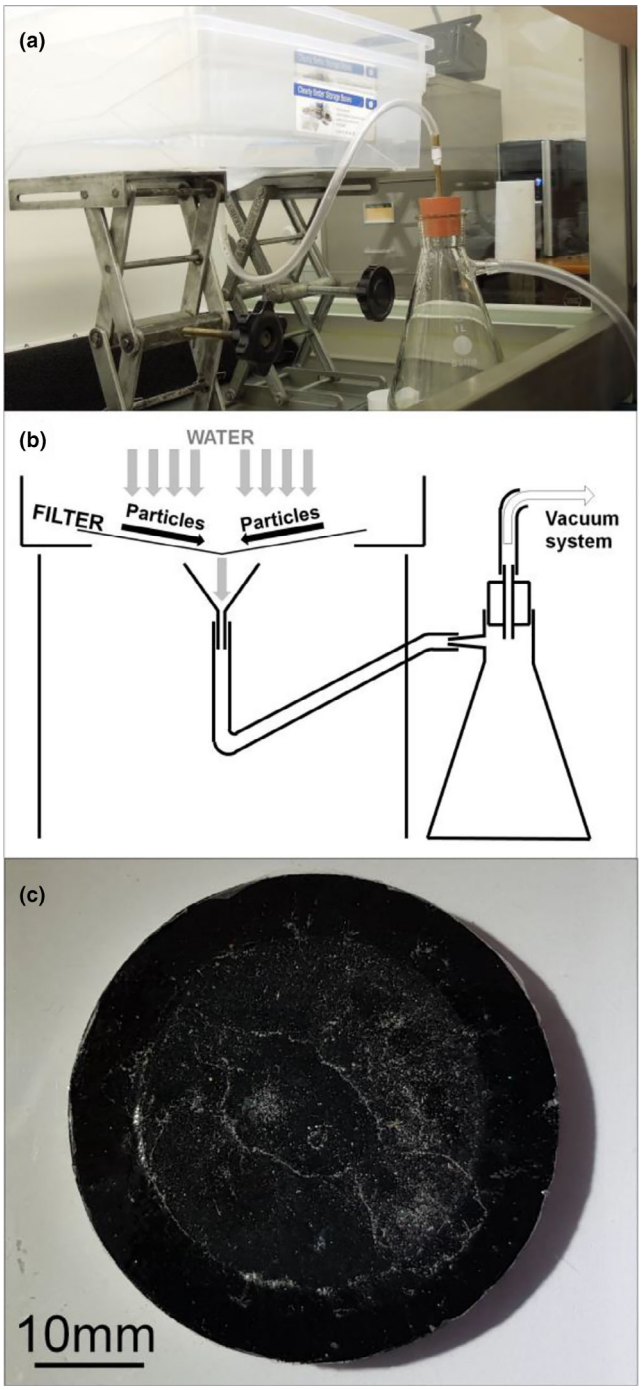

Figure 3. Photo (a) and schematic (b) of apparatus used to wash (remove salt) and concentrate particles on Kwajalein filters. (c) Photo of washed and concentrated filter mounted on SEM stub (with conductive carbon tape) ready for surveying.

Wozniakiewicz et al., 2012). These were dispensed over the filter via a salt-water-particle suspension in order to fix them to the filter with salt upon drying (to replicate the manner in which particles were fixed to the Kwajalein

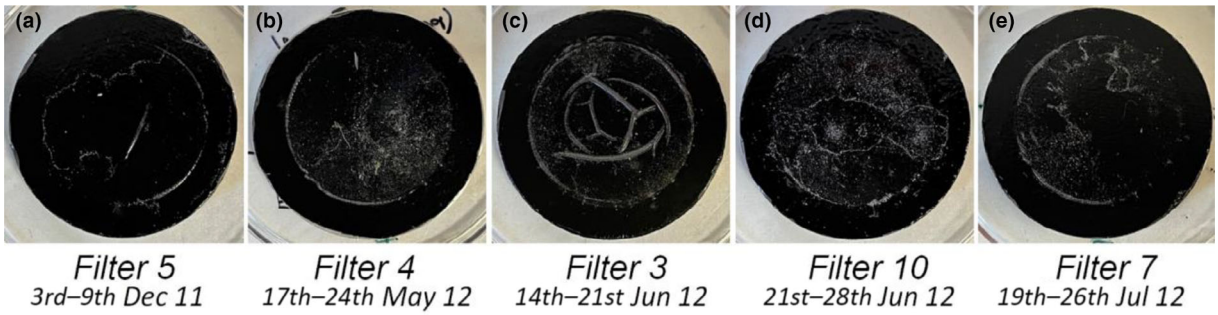

Figure 4. Photographs of all condensed filters showing. (a) Filter 5 (3rd–9th December 2011), (b) Filter 4 (17th–24th May 2012), (c) Filter 3 (14th–21st June 2012), (d) Filter 10 (21st–28th June 2012), and (e) Filter 7 (19th–26th July 2012). Variation in total particle abundance is clearly visible and roughly correlates with spherule abundances summarized in Table 1, with Filter 5 (a) appearing as the least populated, while Filter 10 (d) is the most heavily populated. The curved features visible on Filter 3 (c) are due to wrinkling of the polycarbonate filter as it stuck down on the carbon adhesive tape.

Table 1. Collection details and spherule numbers identified during filter surveys for filters examined in this paper.

Filter No.	Collection period	Area surveyed (mm^2)	Volume of air sampled (m^3)	Number of spherules measured value$_{(normalized\ value)}$					
				Group I	Group II	Group III	Group IV	Multi	Total
5	3rd–9th Dec 2011	263	4279	$8_{(32)}$	$4_{(16)}$	$13_{(51)}$	$1_{(4)}$	$2_{(8)}$	***$28_{(111)}$***
4	17th–24 May 2012	172	4379	$16_{(95)}$	$8_{(47)}$	$29_{(172)}$	$10_{(59)}$	$1_{(6)}$	***$64_{(379)}$***
3	14th–21st Jun 2012	174	3757	$26_{(177)}$	$11_{(75)}$	$57_{(389)}$	$13_{(89)}$	$6_{(41)}$	***$113_{(771)}$***
10	21st–28th Jun 2012	337	3199	$70_{(289)}$	$30_{(124)}$	$18_{(74)}$	$12_{(50)}$	$2_{(8)}$	***$132_{(545)}$***
7	19th–26th Jul 2012	229	2758	$16_{(113)}$	$4_{(28)}$	$28_{(198)}$	$5_{(35)}$	$6_{(42)}$	***$59_{(416)}$***
				$136_{(706)}$	***$57_{(290)}$***	***$145_{(884)}$***	***$41_{(237)}$***	***$17_{(105)}$***	***$396_{(2222)}$***

Note: Filter numbers refer to the order in which filters were prepared and are not related to the dates over which they were exposed for collection. Spherules are categorized into four compositional groups: Group I exhibits a range of compositions designated terrestrial in origin; group II is Fe-rich and contains only additional O, S, and/or Ni; group III is silicate spherules with Mg-to-Si At% ratios less than 0.4; and group IV is silicate spherules with Mg-to-Si At% ratios greater than 0.4. The size ranges observed for each group across the filters were as follows: group I, between 2 and 82 μm; group II, between 2 and 33 μm; group III, between 2 and 58 μm; group IV, between 2 and 38 μm. The size distributions of each group are shown in Figure 8. Several examples of multi-spherule assemblages were identified for each filter, most of which comprise a variety of group III spherules. These are listed separately in the "Multi" column. In total, 396 spherules or spherule-bearing particles have been identified (note that multi-spherule assemblages are counted as a single entry despite being composed of multiple spherules). For each filter studied, the total volume of air that had been sampled varied, as did the amount of the condensed area that was surveyed. Hence, to enable comparison of particle abundances between filters, the values in brackets denote the number of spherules normalized by the ratio of the volume of air sampled to the maximum volume of air sampled by any filter (4379 m^3 by filter 4) and by the ratio of the area surveyed to the total extent of the condensed area (1018 mm^3).

filters). Washing as described above was found to be reasonably efficient at concentrating the particles with minor losses or damage: Using an optical microscope, 151 out of the 156 spheres and all 10 aggregates identified pre-washing were successfully cleaned and concentrated into the concentration zone, with all aggregates remaining intact. Approximately 1 liter of water was applied over the course of ~5 min to wash each filter. No salt crystals were found on the test filters or on the Kwajalein exposed filters during their analysis suggesting that the washing protocol employed had successfully and effectively removed the salt.

Our initial investigation into the Kwajalein samples reported here focuses on five filters with exposure times from 3rd to 9th December 2011 ("Filter 5"), 17th–24th May 2012 ("Filter 4"), 14th–21st June 2012 ("Filter 3"), 21st–28th June 2012 ("Filter 10"), and 19th—26th July 2012 ("Filter 7"). Filter numbers refer to the order in which filters were prepared and are not related to the dates over which they were exposed for collection. After washing and concentrating as described above, the Al stub-mounted filter concentrates were surveyed in the Hitachi S3400 scanning electron microscope (SEM) at the University of Kent. This SEM was operated at 20 kV in variable pressure mode (100 Pa) to enable imaging without the need to apply conductive coatings. All imaging of particles in situ was, therefore, limited to backscattered electron (BSE) imaging on this instrument. Surveys involved acquiring automated image maps at a magnification of ×500 to ensure all particles down to 5 μm (the size of the filter pores and thus the theoretical

lower particle size limit) could be clearly discerned. Despite concentrating particles into a central circular region of ~1 inch diameter, collecting survey maps over this entire area at this magnification proved extremely time-consuming, and therefore, in the interest of investigating more filters in the instrument time available, only nine overnight automated maps of the concentrated sample for each filter were collected and studied. It was intended that these maps should cover one quadrant of the concentrated sample area; however, due to limited and variable instrument time available for individual maps, they varied in size and thus the total area covered varies from filter to filter (see Table 1). Once collected, survey images were reviewed manually to identify particles of potential interest (based on morphology, looking for spherules and fine-grained aggregates or evidence of a magnetite shell). For each of these particles, higher resolution images and energy-dispersive X-ray (EDX) data were obtained in situ to determine whether morphology, surface textures, and chemistry were consistent with extraterrestrial materials. These investigations aimed to identify micrometeorite candidates that require additional analysis as well as common types of contamination (to speed up our later surveys). Once complete, examples of particles deemed to be micrometeorite candidates were removed from the filter, embedded in epoxy resin (Struers SpeciFix-20), and polished to reveal their cross sections for further analysis by SEM (imaging and quantitative EDX) and comparisons with data available for micrometeorites identified in other collections. The resin blocks were C-coated, enabling the study of the particles under vacuum.

In order to obtain quantitative EDX data from the embedded micrometeorite candidates, the instrument was first energy-calibrated with a cobalt standard. Data were also acquired from a polished and C-coated specimen of basalt glass (United States Geological Survey sample NKT-1G) both before and after the analysis sessions to confirm the EDX data being obtained were properly calibrated. All analyses have been calculated by oxygen stoichiometry (i.e., where O is matched to cations assuming all phases present are oxides) and normalized such that their compositional totals equal 100%. In order to obtain data that represented, as closely as possible, the bulk composition of the particle, each spectrum was collected from an area marked out over the entire exposed internal surface of the particle.

RESULTS

Initial Survey Results

Initial low magnification optical and SEM imaging of the filters to produce whole sample maps for location purposes immediately revealed that a large quantity of particles were present on the concentrated samples. During the early survey searches great numbers of particles were identified as of potential interest, having bright appearances (indicating high Z) reminiscent of fusion crust on meteorites, or fluffy aggregate appearances reminiscent of chondritic porous (CP) IDPs. However, higher resolution imaging and compositional analyses revealed that much of this was terrestrial contamination (e.g., coral fragments, sand, rust, soot, and other general detritus). In fact, a far greater number of particles were identified as being of potential interest than it was feasibly possible to obtain higher resolution images and SEM EDX data. Consequently, we chose to focus our efforts on the search for cosmic spherules (CSs). CSs are those particles that undergo melting to form molten droplets during atmospheric entry, forming spherule to sub-spherical shaped particles upon cooling (Genge et al., 2008). They typically exhibit glassy mesostasis with or without microphenocrysts and often also contain vesicles, all characteristics expected for an object that has melted during travel through the atmosphere. CSs exhibit considerable variation in textures, compositions, and mineralogy (Genge et al., 2008; Taylor et al., 2000). Based on mineralogy, they can be broadly subdivided into three groups: iron-rich I-type spherules, silicate-rich S-type spherules and the intermediate G-type spherules. I-type spherules are dominated by the iron oxides wüstite or magnetite, but they can also contain Ni-rich iron metal and occasionally Pt-group element nuggets. G-type spherules are dominated by magnetite dendrites within a silicate mesostasis. S-type spherules are dominated by silicates, with broadly chondritic compositions, but a wide range of textures that allow them to be further subdivided as follows: Glass spherules consist almost entirely of mafic silicate glass; cryptocrystalline (CC) spherules consist of submicron crystallites of silicates and, in many cases, magnetite; barred olivine (BO) spherules are dominated by lathe-shaped olivine crystals within mesostasis which often contain magnetite; porphyritic olivine (PO) spherules are dominated by equant olivine crystals and magnetite crystals within glass; coarse-grained spherules contain >50% relict minerals by volume; CAT spherules have barred olivine textures, Mg/Si ratios greater than 1.7 and, compared with other micrometeorites, are enriched in Ca, Al, and Ti. Based on data from one of the most complete CS collections to date (those collected from the South Pole water well; Taylor et al., 2000), the relative abundances of these different CS types are as follows: 1% I-type, 2% G-type, and 97% S-types, with the latter made up of 41% BO-type, 17% glass type, 12% CC-type, 11% PO-type, 12% relict-grain-bearing spherules (the Taylor et al., 2000 category in which coarse-grained spherules sit) and 1% CAT-type. The remaining 3% were designated scoriaceous-type micrometeorites which exhibit vesicles and relict grains and are considered to represent partially melted particles which are now referred

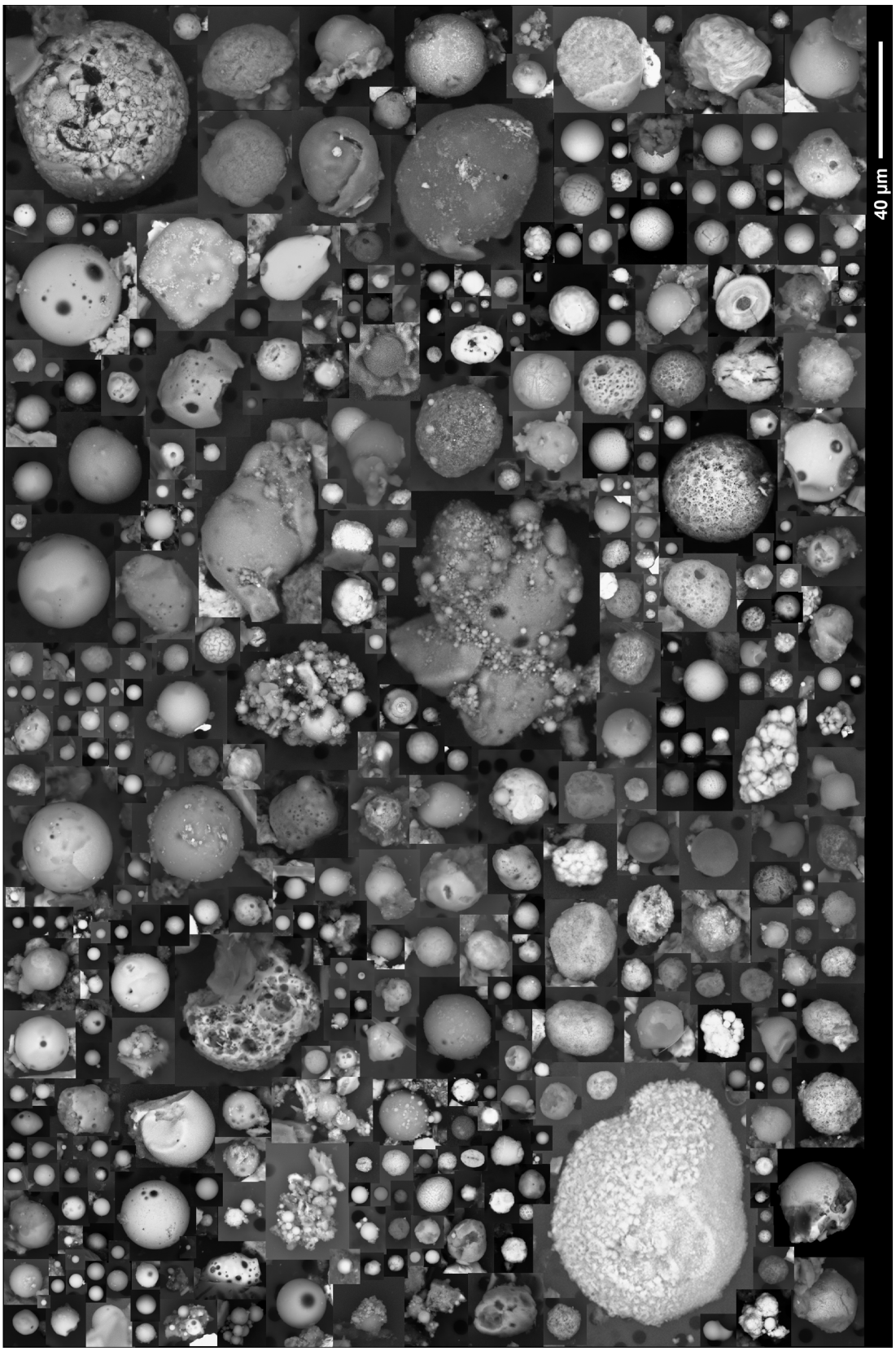

Figure 5. BSE images of all 396 spherules and spherule-bearing particles identified in situ on surveyed areas of Kwajalein filters 3, 4, 5, 7, and 10.

to as a separate category. CSs are suitable targets for this study as they are common in all micrometeorite collections performed to date; their characteristic morphology makes them easy to spot, and they have far fewer terrestrial lookalikes (although, as discussed later, there are still several sources of terrestrial lookalikes that cause complications).

In our SEM survey imaging, a total of 396 spherules or near-spherule-shaped particles ranging in size from ~a few microns up to ~62 μm in diameter were identified (Table 1; Figure 5). The majority of these occurred as single spherules (e.g., Figure 6a–r, v–x), or in some cases multi-spherule assemblages (e.g., Figure 6s–u). Multi-spherule assemblages (referred to as "Multi" in Table 1) were counted as a single particle in these surveys. BSE imaging combined with SEM EDX analyses (performed with particles in situ on filters to provide qualitative chemical data) revealed that these samples exhibit diverse surface textures and compositions; some appear smooth with little to no visible variations in chemistry (based on BSE images contrast and/or the presence of different elements in EDX spectra) while others exhibit clear variations in composition, contain vesicles and/or have rough or textured surfaces (see Figures 5 and 6).

Kwajalein Spherule Types

Spherules were categorized into four compositional groups on the basis of their similarity to cosmic spherules observed in other micrometeorite collections and an understanding (from available literature) of the common types of terrestrial spherules. A decision tree detailing the steps involved in assigning a group to each particle is shown in Figure 7. The first question, whether the particle is a silicate, sought to determine whether the particle could be an S or G-type CS. If not a silicate, the next question asked whether they are Fe-rich and thus potentially an I-type CS. If also not Fe-rich, then the particle was designated as terrestrial in origin and assigned a classification of group I. Those that are Fe-rich were then assessed as to whether they are also rich in elements other than O, S, and Ni, with those that are, being assigned a terrestrial origin and thus group I classification. Those that only contain Fe, O, S, and Ni are classified as group II, which are potentially I-type CSs. For those particles that were deemed silicates in answer to the first question of the decision tree, the Mg to Si ratio was then used to assess their similarity to known CSs. Compositional data available in the literature for common terrestrial sources of silicate spherules suggest that none exhibit an Mg-to-Si ratio (At%) greater than 0.23. For example, volcanic microspherules have Mg-to-Si ratios less than 0.2 (based on data from Lefèvre et al., 1986; Meeker & Hinkley, 1993; Mourne et al., 2007; Spadaro et al., 2002) and fly ash has Mg-to-Si ratio less than 0.23 (based on data from Akyuncu et al., 2018; Bentz, 2014; Bentz & Ferraris, 2010; Law et al., 2015; Lopez-Flores, 1982; Siddique & Khatib, 2010; Sobolev et al., 2014). In contrast, data for silicate-rich CSs suggest that no silicate CSs identified to date exhibit an Mg-to-Si ratio below 0.2 (based on data from Folco & Cordier, 2015 and references therein for G-, and S-type cosmic spherules, and on Taylor et al., 2007 for examples of achondritic cosmic spherules since micrometeorites are not restricted to sampling primitive parent bodies). Given the non-flat sample geometry and thus semi-quantitative nature of the SEM EDX data here, a conservative ratio of Mg/Si = 0.4 was used to distinguish terrestrial silicate-rich spherules designated group III from CS-candidate silicate-rich spherules designated group IV. We note that by using this decision tree, some extraterrestrial spherules may mistakenly be characterized as terrestrial, but the goal here is to focus on those spherules that can be reliably classified as extraterrestrial.

The number of spherules from each group that were identified on the filters is given in Table 1, together with details of the date and duration of sampling, volume of air sampled, and area of filter surveyed. Figure 8 shows the size distribution for the different groups. All groups are dominated (to varying degrees) by spherules in the 5–10 μm size range; however, we note that the filter perforations measure 5 μm across and thus the true abundance of spherules in the 0–5 μm bin is likely higher than shown here since some will have been lost during the collection and washing/concentration process. Backscattered electron images of particles are shown in Figures 5 and 6 and each group is described in more detail below.

Group I

Group I spherules have diverse non-chondritic and non-silicate compositions and include Fe-rich spherules with secondary siderophile elements other than Ni and S (e.g., Al, Cr, or Ti). The most common types of group I spherules are Ca-P-rich (23%), Ca-oxides (15%), Al-oxides (14%), Ti-oxides (9%), Cu-Cl-rich (9%), and Fe-rich oxides (9%). The Ca-P-rich spherules vary in their surface textures, from completely smooth (Figure 6a) to grainy in appearance (Figure 6b) and in some instances, even highly vesiculated (Figure 6c) with clear, rounded voids outcropping on the surface. Nearly all of these (26 out of 31) can be found on one filter—Filter 10—corresponding to a single collection period. The Ca-oxides typically have granular surfaces and are less than 15 μm in diameter (e.g., Figure 6d). One much larger example, which measures ~50 μm in diameter, resembles a rounded conglomerate (Figure 6e). Another apparently broken sphere exhibits internal layering reminiscent of an ooid (Figure 5f). The Al oxides are typically smooth in appearance with most measuring less than 10 μm in diameter (e.g., Figure 6g). The Ti-oxides all exhibit rough (not quite spherical) outlines and their surfaces

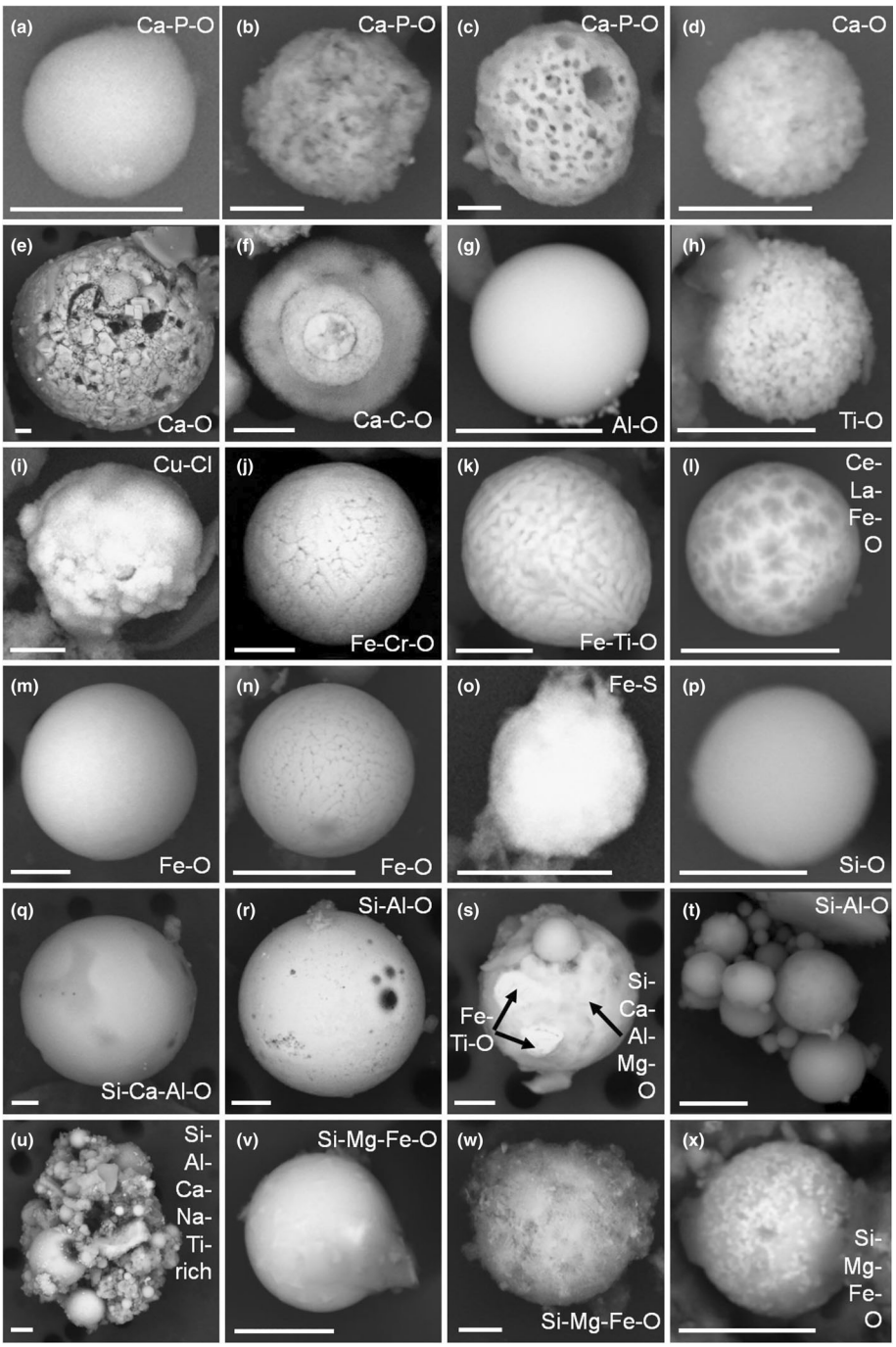

Figure 6. BSE images of examples of different types of spherules identified on Kwajalein filters. A 5-μm scalebar is shown on each image and the major elements present are labeled. (a–l): Spherules deemed to be of terrestrial origin designated group I. (m–o): Fe-rich spherules consistent with I-type spherules but equally similar to Fe-rich spherules of terrestrial origin, designated group II. (p–r): Silicate spherules with Mg to Si ratios less than 0.4 and thus deemed consistent with a fly ash or volcanic origin and designated group III. (s–u): Multi-spherule assemblages, most of which comprise group III spherules. (v–x): Silicate spherules with Mg to Si ratios greater than 0.4 that are deemed CS candidates and designated group IV.

appear granular (e.g., Figure 6h), with most measuring less than 10 μm in diameter. The Cu-Cl-rich particles are typically 10–15 μm in diameter, often exhibit botryoidal textures (e.g., Figure 6i) and are blue when observed optically, consistent with copper sulfate. The Fe-rich oxide spherules commonly contain Cr, Al, or Ti, typically

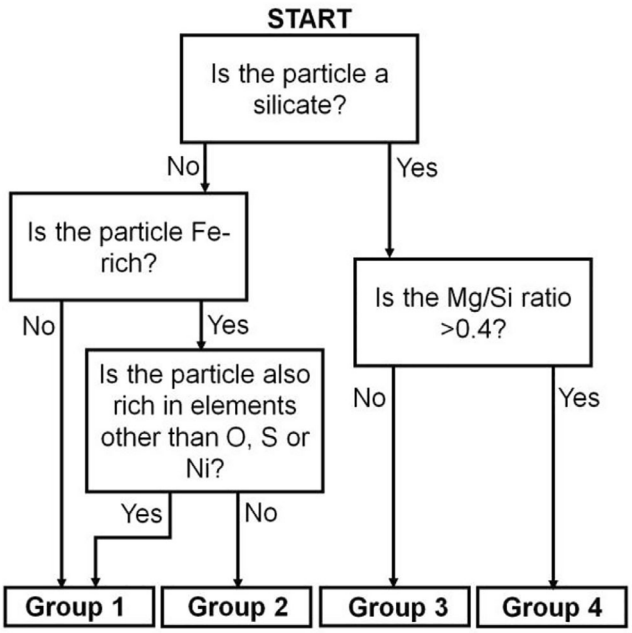

Figure 7. Decision tree used to assign a group to each spherule identified in the Kwajalein collections.

measure between 10 and 15 μm in diameter and have surface textures dominated by interlocking crystals up to a few microns in size (e.g., Figure 6j,k). One curious example measuring a mere ~5 μm in diameter contained the rare earth elements Ce and La (Figure 6l).

Group II

Group II is Fe-rich spherules (e.g., Figure 6m,n) that are mostly oxides but in few cases are sulfides (e.g., Figure 6o). Two are Fe-Ni oxides. The surface textures of group II particles are either smooth (e.g., Figure 6m) or composed of coarse interlocking crystals up to a few microns in size (e.g., Figure 6n) and are similar in appearance to some of the Fe-rich spheres of group I. The Fe oxide spherules exhibit chemistry and morphology consistent with I-type CSs; however, we cannot definitively classify them as extraterrestrial due to their apparent similarity to terrestrially derived Fe-rich spherules. A current lack of appreciable data and understanding of chemical variability amongst these terrestrial sources of Fe oxide spherules to permit comparisons to be made against extraterrestrial I-type particles prevents their distinction and thus the identification of bona fide I-type CSs in these collections. Consequently, the origin of these particles remains uncertain, and must be assumed terrestrial at present. The two Ni-bearing Fe-rich spheres identified under this group, however, could be extraterrestrial in origin; as noted earlier, Ni-bearing iron metal is a distinguishing characteristic of micrometeorites and meteorites (Genge et al., 2008), since anthropogenic Ni-Fe alloys contain other metallic elements (e.g., Co, Mo, Ti, etc. according to the desired material properties). Indeed, the ratio of Ni-Fe spherules in group II to S-type candidates in group IV found here is slightly higher than that reported for the South Pole water well (~0.05 here compared to ~0.01 reported in Taylor et al., 2000); thus, quantitative chemical analysis would be required to confirm the composition and examine the particle further. Unfortunately, due to their small size (only ~5 and 6.5 μm in diameter), they proved too small to handpick from the filter for further study here.

Group III

Group III spherules (e.g., Figure 6p–r) have compositions rich in Si and O. Some exhibit compositions dominated by only these two elements (e.g., Figure 6p) but often they also contain high abundances of Al, Ca, Na, and/or K (e.g., Figure 6q,r). These spherules vary considerably in appearance as well as composition, from perfectly smooth and homogenous (e.g., Figure 6p), to multi-component (Figure 6q), vesiculated (e.g., Figure 6r) and sometimes with outcropping mineral grains (e.g., Figure 6s). The majority of multi-spherule assemblages also fall into this group (e.g., Figure 6s–u).

Group IV

Group IV spherules are those spherules that we have identified, using our conservative decision tree, as being CS candidates (e.g., Figure 6v–x). Their bulk chemistry is dominated by Mg-rich silicates, often accompanied by high Fe content and, in some cases, Ca content. These also display a variety of surface morphologies, with several exhibiting distinct bright crystallites, often with cross or pyramid morphologies characteristic of magnetite as observed on CSs in other collections. Others appear to have vesicles outcropping on their surfaces.

The combination of textures and chemistries exhibited by group IV particles are significantly different from known examples of terrestrial spherules. Thus, examples were picked and prepared for further, more detailed examination by SEM as described in the next section. The potential origins of group I, II, and III particles are considered later in the discussion section of this paper.

Detailed Study of Group IV Candidate CSs

Seven spherules from group IV with apparent chondritic compositions and, in some cases, external textures observed on cosmic spherules identified in other micrometeorite collections, were chosen for further study. These ranged in size from 8.5 μm to 35.4 μm in diameter (the sizes of each individual particle are provided in Table 2). Images of each particle's exterior (taken in situ on filters) and interior (taken after picking, embedding in

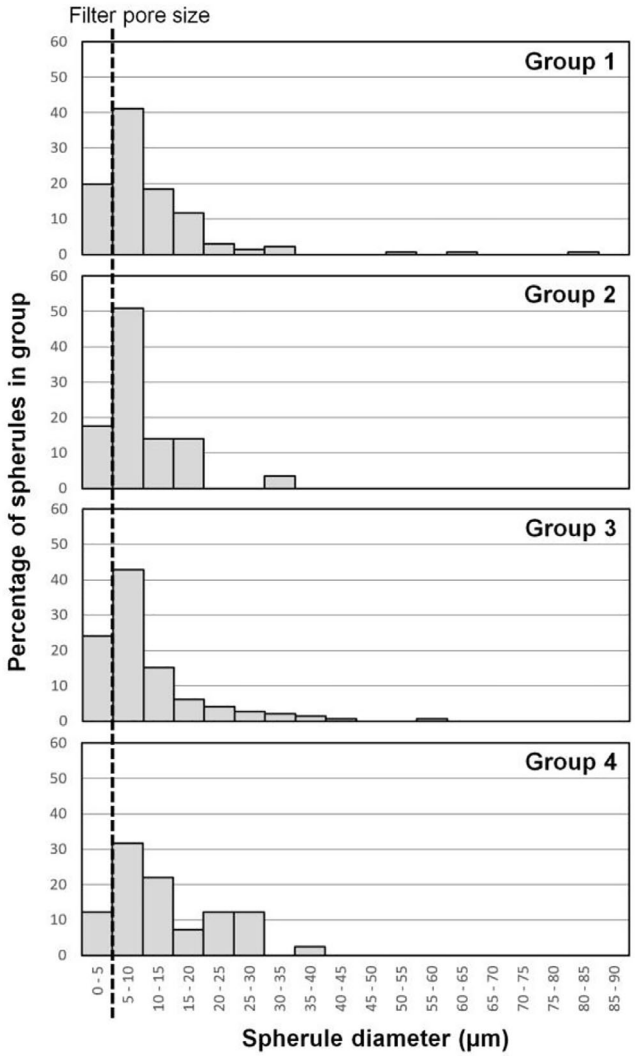

Figure 8. Spherule size distributions for each of the four groups of spherules identified. Individual spherule sizes are diameters measured in micrometer from high-magnification SEM images of each. The number of spherules in each size bin is expressed as a percentage of the total number of spherules in that group. These distributions suggest a peak in abundance of 5–10 μm spherules for all four spherule groups. We note, however, that sampling is likely biased toward this particular size range, since smaller particles are drawn into the vacuum system from further away than larger particles, and particles smaller than 5 μm in diameter (represented by the black dashed line) are smaller than the filter perforations, and therefore, can be lost during collection or washing/concentrating of the filter.

resin, and polishing through to reveal cross sections) are shown in Figure 9. Bulk atomic percentage (At%) data collected from the now flat and C-coated specimens are tabulated for each spherule in Table 2. These data have been calculated by oxygen stoichiometry and normalized such that their compositional totals equal 100%. The nomenclature used for picked particles is as follows: *F [filter number prepared]_M[map number]_S/P [sphere/particle number]*.

Bulk EDX At% data obtained for these particles (from flat polished sections) are plotted on ternary diagrams in Figure 10 together with compositional data taken from the literature for the various types of cosmic spherule micrometeorites (Folco & Cordier, 2015 and references therein for I-, G-, and S-type cosmic spherules and Taylor et al., 2007 for achondritic cosmic spherules). Given that many micrometeorites are believed to be derived from chondritic parent bodies, data are also plotted for chondritic meteorites (Hutchison, 2004 and references therein). These data include both bulk compositions, and average compositions for individual chondritic meteorite components (i.e., the average chondrule, average CAIs, and average matrix composition for different chondrite types) since the small size of micrometeorites is more akin to a single or few individual components of meteorites rather than bulk samples. Compositional data for volcanically derived spherules (taken from Lefèvre et al., 1986; Meeker & Hinkley, 1993; Mourne et al., 2007; Spadaro et al., 2002) and fly ash (taken from Akyuncu et al., 2018; Bentz, 2014; Bentz & Ferraris, 2010; Law et al., 2015; Lopez-Flores, 1982; Siddique & Khatib, 2010; Sobolev et al., 2014) are also included for comparison as the most abundant type of terrestrial spherule with similarities to S and G-type CSs. All seven particles studied in detail here plot amongst the cosmic spherule and meteorite data in Figure 10, and importantly, although some do not plot consistently with the same type of extraterrestrial material on both ternaries, they remain outside the regions occupied by volcanic spherules and fly ash.

The compositions of our candidate particles are examined further in Figure 11 by comparing their silicon- and CI-normalized elemental compositions with those of S- and G-type CSs and achondritic CSs in Figure 11b, with bulk chondrites and chondrite components in Figure 11c, and with those of volcanic and silicate fly ash spherules in Figure 11d. All data are from the same sources as used in Figure 10. None of the Kwajalein particles plots entirely within the range exhibited by chondritic CSs, although in nearly all cases, those elements fall within the ranges of other extraterrestrial materials plotted on Figure 11b,c. We also note, however, that when compared against the data available for volcanic and silicate fly ash spheres, there is a clear discrepancy for Mg and Fe (as also observed in Figure 10a). These are two of the three major elements (along with Si) observed in CSs and thus the most critical chemical markers to match. A terrestrial origin, therefore, seems implausible based on the currently available data for terrestrial sources of spherules.

As noted in the methods section, particles on the filters had sat in salt water for a period of up to 18 months before producing the observed salt coating once they were dried

Table 2. Bulk At% data obtained by SEM–EDX for the seven Kwajalein candidates that were embedded in resin and polished flat to expose their interiors.

Candidate (size) Element	F3_M7_S30 (~12 μm)	F3_M7_S7 (~27 μm)	F4_M1_S210 (~8 μm)	F4_M6_S4 (~38 μm)	F7_M2_S10 (29 μm)	F10_M9_S6 (~24 μm)	F10_M6_P2 (~22 μm)
O	57.3	57.9	57.1	56.3	57.1	57.6	59.5
Na	1.3	1.0	0.3	0.1	0.2	1.0	0.3
Mg	12.8	13.1	11.3	8.8	15.3	8.5	7.4
Al	0.6	2.1	0.9	6.8	0.2	2.8	3.0
Si	14.9	15.3	14.1	8.5	14.3	14.1	16.1
P				0.3		0.1	0.3
S				0.3			0.2
Cl	0.1		0.3	0.8			1.2
K	0.2	0.2			0.1	0.1	0.1
Ca	1.5	1.4	7.4	6.2	0.9	7.6	2.7
Ti	0.1		0.1	0.6		0.3	2.0
Mn	0.1	0.1	0.1	0.2	0.1	0.1	0.3
Fe	11.0	8.9	8.4	10.8	11.7	7.7	6.1
Ni	0.1	0.1		0.1	0.1		0.1
Cu							0.1
Zn				0.3			0.6
Total	99.9	100.1	100	100.1	100	99.9	100

Note: The size (average diameter in micrometer) derived from images taken while in situ on the filter (prior to picking and embedding in resin) is noted beneath each particle. All EDX analyses have been normalized to oxygen stoichiometry (i.e., where O is matched to cations assuming all phases present are oxides). In order to obtain data that represented, as closely as possible, the bulk composition of the particle, each spectrum was collected from an area marked out over the entire exposed internal surface of the particle. Chlorine is observed in four particles, most notably in two which have internal voids (F4_M6_S4 and F10_M6_P2) that may have filled with resin which contains Cl (infilling with salt was considered as an explanation for this Cl; however, no associated increase in Na is observed, thus this was discounted as an explanation). These two particles also exhibit small amounts of Cu and Zn, that again may be contaminants which have invaded their porous structures (e.g., during the filter preparation process).

out. This had to be removed prior to filter analysis, and consequently the washing method employed could potentially have weathered and leached the particles. Indeed, during our initial in situ examination of the candidate CSs studied here, some did appear to have small amounts of material typically rich in Si, Ca, and Al attached to their surfaces (see Figure 9). On embedding in resin and polishing through, five of the particles appeared largely solid (F3_M7_S30, F3_M7_S7, F4_M1_S210, F7_M2_S10 and F10_M9_S6) while two were highly porous (F4_M6_S4 and F10_M6_P2). The rims of the five solid particles remained well defined with no evidence of loss of glassy constituents (as observed, e.g., in weathered CSs from the Antarctic, e.g., van Ginneken et al., 2016). Bulk analyses obtained with care taken to avoid including the contamination coatings should, therefore, be representative of an unaltered particle. For the two highly porous particles, however, it is possible that salt water or water from the washing process (potentially carrying minute particles or dissolved matter from elsewhere on filter) may have entered and deposited material within. Both Cu and Zn were observed in the porous particles (Table 2) and are believed to originate from such contamination and thus have not been plotted in Figure 10. Similarly, data for Cl are included in Table 2, but are not plotted in Figure 10 as this is believed to be at least partly contributed to by the embedding resin; again, the two particles that exhibit the highest Cl are the highly porous F4_M6_S4 and F10_M6_P2 since their pores have been infilled by the embedding resin, and thus their bulk analyses will contain contributions from it.

Each Kwajalein candidate shown in Figure 9 is now described individually in more detail below.

F3_M7_S30

F3_M7_S30 is a spherical particle measuring ~12 μm in diameter. Externally, this particle is covered in bright (high Z) dendrites with a mixture of triangular and cross-shaped outlines in a darker smooth matrix. The dendrites are 1–2 μm in size and have pointed peaks at their centers that protrude beyond the matrix creating a surface covered in prominences. Internally, we see that the dendrites extend throughout the particle. EDX data suggest that the dendrites are Fe-oxides surrounded by a silicate matrix that varies in composition from Mg-rich to Mg-Ca-rich silicates. The external texture of this particle appears similar to that of G-type CSs, although once sectioned the abundance of silicate matrix appears higher and the particle appears most similar in appearance to porphyritic (Po) or micro-porphyritic (μPo) S-type CSs (as

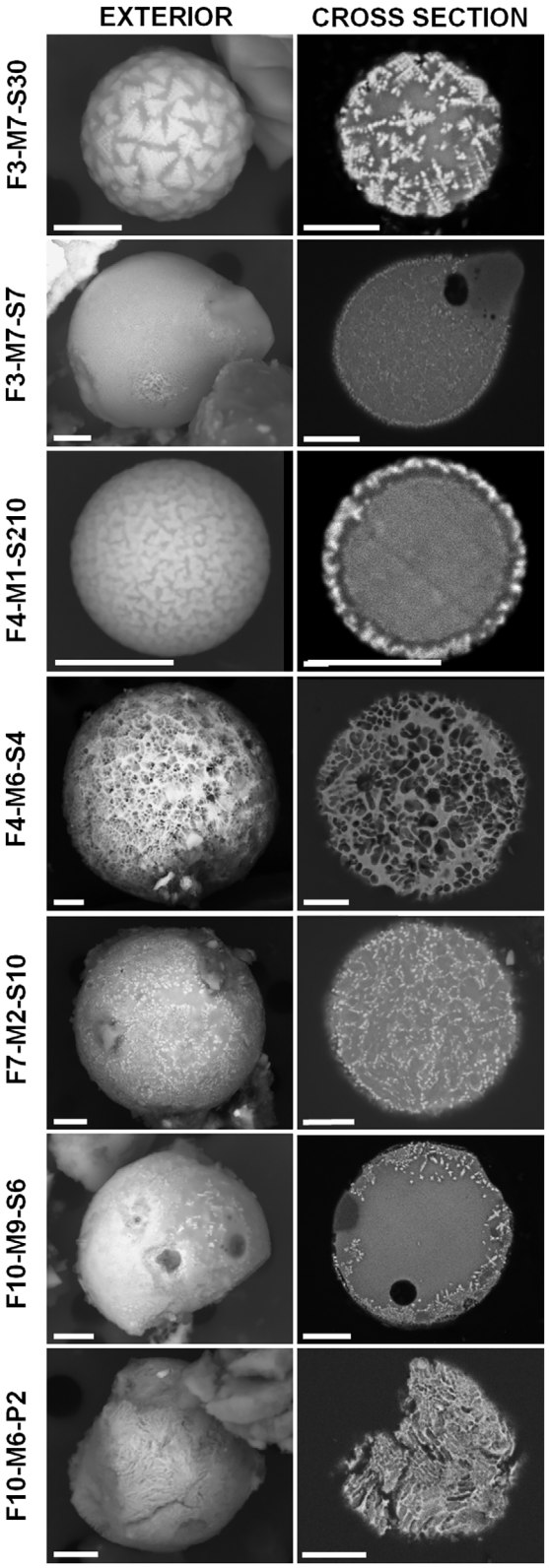

Figure 9. BSE images of exterior (left-hand side images obtained in situ on filter) and interior (right-hand side images obtained after picking, embedding in resin, and polishing) of seven cosmic spherule candidates identified on surveyed areas of Kwajalein filters 3, 4, 7, and 10. All scale bars are 5 μm.

individual grains within this particle are larger than ~1 μm). Indeed, on the ternary diagrams of Figure 10, the bulk composition of this particle departs from that of G-type CSs, being lower in Fe, and instead plotting closer to S-type CSs, amongst (Figure 10a) or close to (Figure 10b) bulk chondrites and matrix. Figure 11 shows that the composition of the particle plots within the range exhibited by S- and G-type CSs for most elements, but is slightly higher in Na and K and has no detectable S or P. The values for these elements, however, are within the range exhibited by chondrites or chondritic components and thus remain consistent with an extraterrestrial origin. Based on its composition and texture, we classify this particle as extraterrestrial in origin, most akin in appearance to a porphyritic S-type CS.

F3_M7_S7

F3_M7_S7 is droplet shaped, measuring ~27 μm along its longest dimension. Externally, the surface of the body of the droplet appears speckled, with bright, similarly sized crystallites in a darker matrix. In contrast, the tail of the droplet appears smooth, with one angular edge apparent and with no crystallites outcropping on the surface. Internally, we see that the droplet is composed of two parts. The first comprises the main body of the droplet, exhibiting the same sub-micron bright crystallites in a darker matrix as observed externally, although the crystallites appear concentrated at the surface. The second is the tail of the particle which contains no crystallites and appears darker in BSE images compared to the matrix of the droplet body. EDX data suggest that the bright crystallites are Fe-oxides with the main body of the droplet being Mg-rich silicate and the tail being Al-Ca-rich silicate. Given the sharp edge of the Al-Ca-rich silicate tail when viewed externally, it is possible that this is a relict grain. Relict grains are observed in CSs, particularly those <250 μm in diameter, and although they are typically olivines or pyroxenes, other compositions including anorthite (an Al-Ca-rich silicate) have previously been observed (Taylor et al., 2012). Vesicles are also present at the boundary between the Mg-rich and Al-Ca-rich silicate. The occurrence of the Al-Ca-rich silicate in the tail is reminiscent of density-driven migration of components

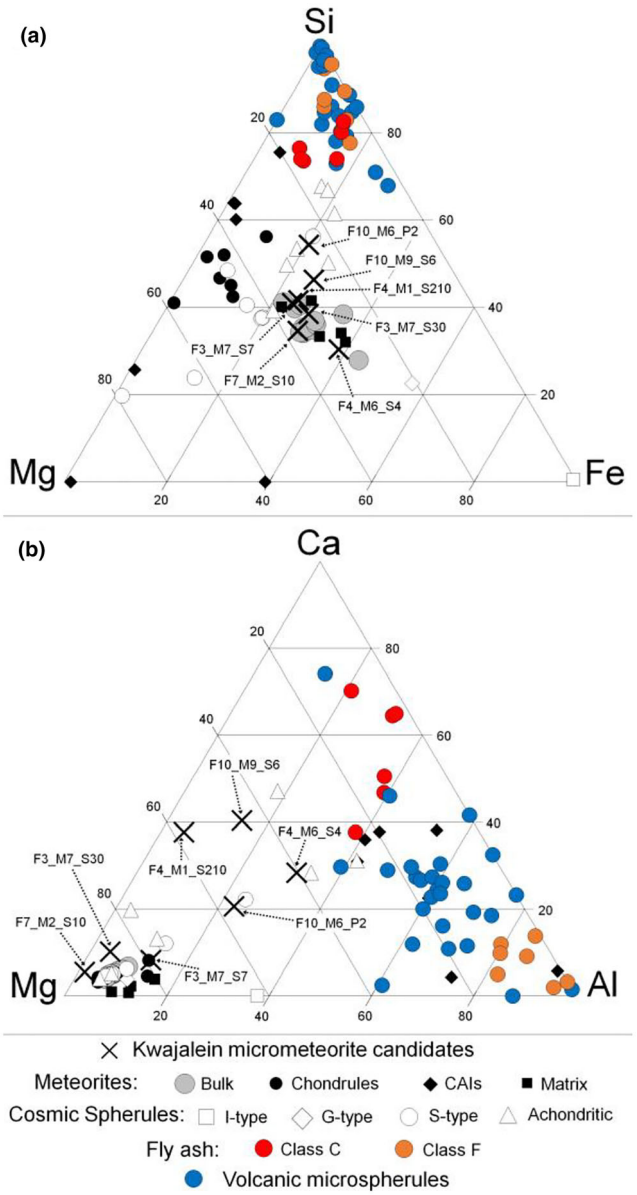

Figure 10. Ternary diagrams displaying relative abundances of (a) Mg, Si, and Fe and (b). Mg, Ca, and Al based on At% compositional data for Kwajalein CS candidates plotted against average compositional data from literature for different classes of cosmic spherule micrometeorites (Folco & Cordier, 2015 and references therein) and for bulk and main components of chondritic meteorites (Hutchison, 2004 and references therein). Micrometeorite data for S-type cosmic spherules include individual data points for cryptocrystalline, barred olivine, porphyritic, and glassy spherule sub-types. Data from several studies in the literature have also been plotted for volcanic microspherules (Lefèvre et al., 1986; Meeker & Hinkley, 1993; Mourne et al., 2007; Spadaro et al., 2002) and fly ash (Akyuncu et al., 2018; Bentz, 2014; Bentz & Ferraris, 2010; Law et al., 2015; Lopez-Flores, 1982; Siddique & Khatib, 2010; Sobolev et al., 2014) to show our candidate cosmic spherules plot away from these common terrestrial contaminants.

which has previously been observed in CSs (Genge et al., 2016). The bulk composition of this particle plots amongst, or close to, S-type CSs on the ternary diagrams in Figure 10. Figure 11 shows that the composition of the particle plots within the range exhibited by S- and G-type CSs for most elements, but is slightly enriched in Na and K and has no detectable S, P, or Ti. The values for Na and K, and the missing S and P are, however, within the ranges exhibited by chondrites or chondritic components and thus remain consistent with an extraterrestrial origin. Titanium can be a minor constituent of CSs and thus its non-detection could be a result of an abundance below the detection limit of this instrument. Based on its composition and texture, we classify this particle as extraterrestrial in origin, most akin in appearance to a cryptocrystalline S-type CS.

F4_M6_S4

F4_M6_S4 is a spherical particle measuring ~38 μm in diameter. This particle is unusual in its appearance and unlike any CS identified to date, being extremely vesiculated throughout, with individual vesicles measuring ~500 nm to 2 μm in diameter. EDX data show that the particle is dominated by Fe, Si, Mg, Al, and Ca, and that the particle is not homogenous in composition, with one half being Mg-rich silicate and the other Ca-rich silicate. It also appears to contain small (~100 nm), higher Z crystallites which EDX data suggests are enriched in Ca relative to the rest of the particle. Compositionally this particle is more enriched in Fe compared with S-type CSs, plotting amongst bulk chondrites and matrix on the ternary diagrams of At% Mg:Si:Fe (Figure 10a). It is also more enriched in Ca and Al than S-type CSs, plotting closer to achondritic CS compositions on the ternary diagram of At% Ca:Mg:Al (Figure 10b). Looking in more detail at its composition in Figure 11, this particle is slightly enriched in Al, P, S, Ca, and Ti compared with S- and G-type CSs and it exhibits no K. Of these elements, S is within the range observed for chondrites and Al, Ca, and Ti are within the range observed in CAIs, while K is also a minor constituent of CSs and its non-detection could be a result of an abundance below the detection limit of this instrument. However, P is enriched compared with the extraterrestrial samples plotted and instead sits within the range observed in volcanic spheres. We also note the presence of minor amounts of Zn which has not been reported previously in micrometeorites. As noted earlier, however, given the porous nature of this particle, it is possible this is terrestrial contamination (from elsewhere on the filter) that has made its way into the particle during the filter preparation procedure (washing). Given its unusual morphology (not observed previously in CSs or, as far as the authors can determine from literature,

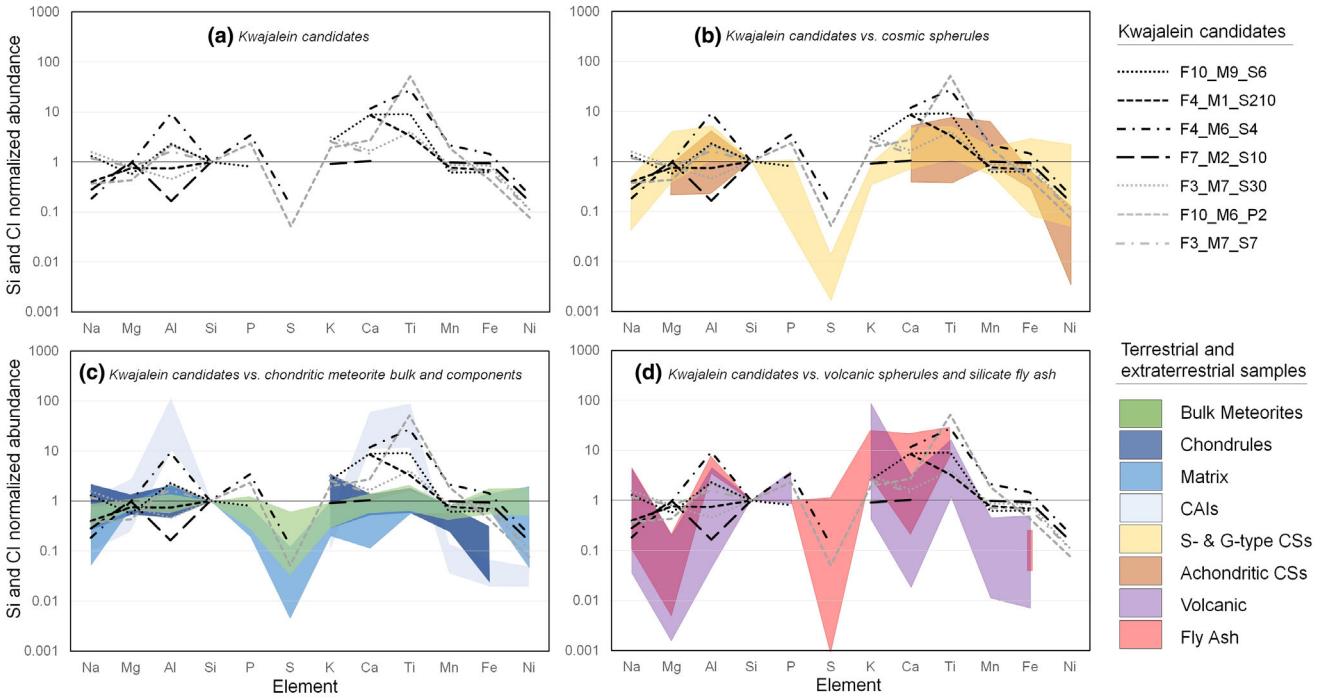

Figure 11. Si- and CI-normalized abundances of major elements for the Kwajalein CS candidates (a). For comparison, these have been plotted overlying (b) the range observed for S- and G-type cosmic spherule micrometeorites (Folco & Cordier, 2015 and references therein) and achondritic cosmic spherule micrometeorites (Taylor et al., 2007), (c) the range observed for the bulk and main components of chondritic meteorites (Hutchison, 2004 and references therein), and (d) the range observed for terrestrial fly ash (silicate dominated class C and F) and volcanic spherules (for data sources see for Figure 10).

in terrestrial samples either) and given that it does not have Mg or Fe contents consistent volcanic spheres, yet is enriched in P compared with extraterrestrial samples, it is not possible to assign an origin to this particle. We note, however, that two other particles with similar appearance and composition were also identified on the same filter (Filter 4), thus *if* extraterrestrial in origin, they represent a new type of particle, likely from the same source and linked to some transient event.

F4_M1_S210

F4_M1_S210 is a spherical particle measuring ~8 μm in diameter. Externally, its surface appearance is similar to that of F3_M7_S30, being covered in bright (high Z) crystallites with a mixture of cruciform outlines, although these are smaller (<1 μm) and more densely packed, with less outcropping interstitial smooth matrix. Internally, the crystallites are concentrated at the surface, making a very well-defined bright (high Z) rim surrounding a darker core. EDX data suggest that the bright crystallites are Fe-oxides while the interior is an Mg-Ca-rich silicate. Partial metal and magnetite rims have been reported for larger (>55 μm diameter) cosmic spherules, thought to be the result of metal segregation upon melting, followed by its migration as a bead to the surface whereupon it wets the particle exterior and, if retained within a cavity, may oxidize (Suttle et al., 2021). The complete coverage combined with uniform thickness of the rim on F4_M1_S210 is unusual but may stem from a large metal-to-silicate ratio originally contained within this particle, or an alternative mechanism of formation due to the different size scales involved. Toward the surface, there appears to be very fine bright crystallites just visible at the resolution afforded by this microscope. Thus, we suspect that there may be small crystallites throughout this apparently smooth material. Compositionally this particle plots close to S-type CSs (amongst bulk chondrites and matrix) on the ternary diagram of At% Mg:Si:Fe (Figure 10a), and in the region occupied by achondritic CS compositions, albeit depleted in Al, on the ternary diagram of At% Ca:Mg:Al (Figure 10b). Figure 11 shows that the composition of the particle compared with that of S- and G-type CSs is slightly depleted in Al and slightly enriched in Ca compared with that of S- and G-type CSs, and has no detectable S, P, K, or Ni. Although deviating from CS compositions, the Al lies within the range exhibited by chondrites, and the Ca lies between that exhibited for CAIs and chondrules. The lack of S, P, and Ni remains consistent with the data exhibited for chondritic components (chondrules) while K is also a minor constituent of CSs, and

its non-detection could be a result of an abundance below the detection limit of this instrument. Its composition thus remains consistent with an extraterrestrial origin. Based on its composition and texture, we, therefore, classify this particle as extraterrestrial in origin, most akin in appearance to a cryptocrystalline S-type CS, albeit with an unusually thick (relative to its size) magnetite rim.

F7_M2_S10

F7_M2_S10 is a spherical particle measuring ~29 μm in diameter. This particle is composed throughout of bright (high Z) crystallites in a darker smooth matrix—similar in appearance to the main body of particle F3_M7_S7 but with slightly larger crystals. EDX data suggest that the crystallites are Fe-oxides surrounded by Mg-rich silicate. The bulk composition of this particle plots close to S-type CSs on the ternary diagrams of Figure 10. Figure 11 shows that the composition of the particle plots within the range exhibited by S- and G-type CSs for most elements, but is slightly depleted in Al and has no detectable S, P, or Ti. Although deviating from CS compositions, the lack of S and P remains consistent with the data exhibited for chondritic components (chondrules). The lack of Ti is not consistent with any of the plotted extraterrestrial or terrestrial data but, since Ti is commonly a minor constituent of CSs, this could simply be a result of the detection limit of this instrument. The Al value lies just beyond the range exhibited for achondritic CSs and is thus not consistent with any of the plotted extraterrestrial samples. Given its similarity in appearance and composition to the body of F3_M7_S7, however, we propose that this particle is also extraterrestrial in origin (merely lacking the relict Al-silicate grain that would increase its Al-content to within the S-type CS range) and is most akin in appearance to a cryptocrystalline S-type CS.

F10_M9_S6

F10_M9_S6 is a broken sphere measuring ~24 μm in diameter. Externally, the particle appears to have two halves, with one side bright (high Z) and smooth and the other a mixture of bright (high Z) crystallites in a darker matrix. Several vesicles are also observed outcropping on the surface. Internally, the particle appears to have a core of smoother material with bright crystallites, several with cross-shaped outcrops, concentrated toward the edges. EDX data suggest that the crystallites are Fe-oxides, and the smooth material is Mg-Ca-rich silicate. A single vesicle is observed internally and at one edge of the particle is a relict Al-Ca-rich silicate grain (appearing darker in the BSE image than the surrounding Mg-Ca-rich silicate) similar to that comprising the tail of M3_S7_M7. Compositionally this particle plots between S-type CSs and achondritic CSs on the ternary diagram of At% Mg:Si:Fe, and within the region occupied by achondritic CSs and with one nearby S-type CS on the ternary diagram of At% Mg:Ca:Al Figure 10. Figure 11 shows that the composition of the particle compared with that of S- and G-type CSs is enriched in Na, K, Ca, and Ti with no detectable S. Although deviating from the CS compositions, the data for these elements lie within, or between, the ranges exhibited for chondritic components (chondrules and CAIs) and the lack of S also remains consistent with some chondritic components (chondrules). Based on its composition and textures, we classify this particle as extraterrestrial in origin, most akin in appearance to a cryptocrystalline S-type CS.

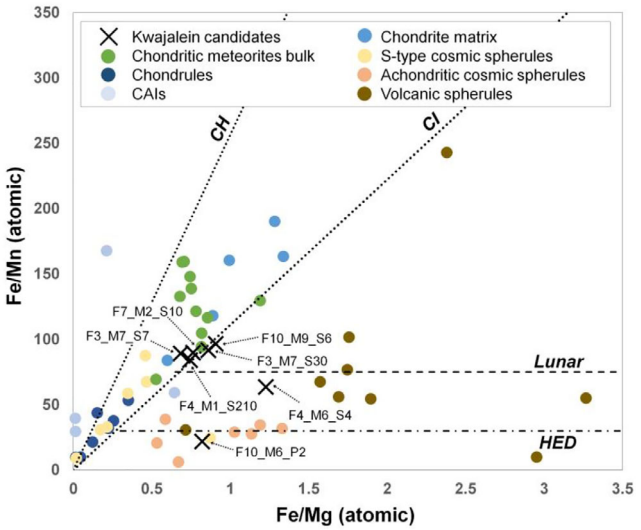

Figure 12. Mn-Mg-Fe systematics for Kwajalein CS candidates studied in detail compared to that of bulk and main components of chondritic meteorites (Hutchison, 2004 and references therein), S-type cosmic spherules (Folco & Cordier, 2015 and references therein), and achondritic cosmic spherules (Taylor et al., 2007). For comparison, data for volcanic microspherules are also included (for sources see Figure 10). Fly ash is not plotted since none of the data referred to previously in Figure 10 contained detectable Mn. Lines are also plotted for CI and CH chondrites (to show the range reported for carbonaceous chondrites), and for the HED and Lunar meteorites (Goodrich & Delaney, 2000). Five of the Kwajalein candidates identified as extraterrestrial CSs plot close to the CI line.

F10_M6_P2

F10_M6_P2 is another broken spherule ~22 μm in diameter. This particle's appearance is unlike CSs identified to date, with an external surface that appears almost fibrous and cracked and with similar textures observed internally. Compositionally the particle appears homogenous, being Mg-rich silicate and with a bulk composition that plots amongst chondritic and achondritic CSs on the ternary diagrams of Figure 10. Figure 11 shows that the composition of the particle compared with that of S- and G-type CSs is highly enriched in Ti, with slight enrichments in

P, S, and K. Although deviating from the CS compositions, the data for S are within the range for bulk chondrites, K is within the range for chondrules, and Ti is within the range for CAIs. Phosphorous, however, is enriched compared with both extraterrestrial and terrestrial samples included here. We also note the presence of trace amounts of Zn and Cu which is inconsistent with extraterrestrial origin, although given the fibrous, perhaps porous nature of this particle. Again we suggest it is possible that this is terrestrial contamination (from elsewhere on the filter) that has made its way into the particle during the filter preparation procedure (as also noted for F4_M6_S4). Given this composition combined with its unusual appearance, it is not possible to assign an origin to this particle. We note, however, that several particles designated as group IV spherules with similar textures were observed on other filters, thus *if* extraterrestrial in origin, they represent a new type of particle that is relatively common in such collections.

To further explore the chemistry of the Kwajalein candidates and determine their origins, a plot of atomic Fe/Mn ratios against Fe/Mg ratio was created (Figure 12). Mn-Mg-Fe systematics have been used previously to explore variations between chondritic and achondritic meteorites; Goodrich and Delaney (2000) showed that chondritic meteorites lie within a well constrained triangular region defined by two straight lines passing through the origin of an Fe/Mn ratio versus Fe/Mg ratio plot, while achondritic meteorites sit on roughly horizontal arrays. Taylor et al. (2007) later applied this to their analyses of chondritic (S- and G-types) and suspected achondritic CSs from South Pole water well collections, arguing that extending the use of Mn-Mg-Fe systematics to the smaller micrometeorites was possible because, despite their smaller size and extensive heating during atmospheric entry, neither Mn nor Mg are subject to loss (e.g., via preferential loss upon evaporation) while the loss of Fe that commonly occurs as metal (through segregation, migration, and ultimately, loss of metal beads from CSs) would merely shift their data point directly toward the origin. The authors found that the chondritic CSs sat within the triangular region with chondritic meteorites, while their achondritic CSs did indeed sit on a roughly horizontal array with HED meteorites. Mn-Mg-Fe systematics were also used by Cordier et al. (2011) to identify five more achondritic CSs in South Pole water well and Transantarctic Mountain collections. Plotting the data for our seven Kwajalein particles in Figure 12, we find that the five spherules we have identified above as extraterrestrial in origin also plot on the edge of the triangular region with chondritic meteorites and chondritic CSs. Although our two particles of unknown origin plot close to the HED (F10_M6_P2) or Lunar trendlines (F4_M6_S4), we cannot assign such an origin given that the terrestrial volcanic microspherules also plot on these lines (as shown in Figure 12) and, thus, a terrestrial origin cannot be excluded by this study.

Confirmation of a lunar origin for F4_M6_S4 would be particularly interesting, as it would represent the first such micrometeorite. The study of isotopic systems is often invoked to assist in linking/distinguishing the origins of meteorites and micrometeorites; however, most studies suggest that the Moon is indistinguishable from the Earth for most commonly used isotopic systems (e.g., oxygen; Young et al., 2016; titanium, Zhang et al., 2012; chromium, Lugmair & Shukolyukov, 1998, etc.). Some more recent high-precision studies have shown that there may be differences for a least some samples, for example, oxygen isotope studies of a range of lunar rock types by Cano et al. (2020) revealed that lunar mantle-derived samples are more distinct from the Earth. Unfortunately, however, an issue with F4_M6_S4 (and indeed, F10_M6_P2) is that it is melt-derived, small and highly porous, and appears to have incorporated resin from the embedding medium during preparation, meaning such analyses would likely be compromised with regard to isotopic measurements. The sample has been preserved for future studies. Perhaps our best hope of linking these, or any other micrometeorites, to the Moon lies in the future with the Lunar Gateway whose anticipated dust experiments will aim to study the lunar dust environment, including lunar ejecta (Wozniakiewicz et al., 2021).

DISCUSSION

Of the seven group IV spherules studied in more detail, five were identified as extraterrestrial CSs, being most similar to S-type CSs. Of these, four were designated as most similar to cryptocrystalline S-type CSs, and one as most similar to porphyritic or micro-porphyritic S-type CSs. This is at odds with the findings from studies of other collections, where the dominant S-type CSs are by far the barred olivine sub-type (e.g., Taylor et al., 2000). We also note that none of the particle compositions match exactly with those of previously studied CSs and that of these five particles, two appear to exhibit an Al-Ca-rich silicate relict grain, something only rarely observed in S-type CSs (e.g., Taylor et al., 2012). Observing differences like these should, perhaps, come as no surprise, given that the majority of CS studies performed to date have only considered particles larger than 50 μm in diameter. All of the Kwajalein CS candidates identified here are <50 μm in diameter, and thus, it could be argued that differences observed between these, and previously identified CSs, are linked to their smaller size. For example, while particles >>50 μm may sample multiple components and exhibit close to bulk

chondritic compositions, particles >50 μm may sample whole individual components (e.g., whole chondrules) and exhibit close to chondritic component compositions, but particles <50 μm are more likely to sub-sample individual components and depart from even individual chondritic component compositions. One study that did focus on the smaller, 25–50 μm fraction of particles, was that of Gounelle et al. (2005). The authors extracted seven cosmic spherules from Antarctic ice at Cap Prudhomme. Bulk chemical data were obtained for three of these, exhibiting a wide range of compositions deemed by the authors to be compatible with larger cosmic spherules. However, this is a very limited number of small spherules and further studies are needed to build a robust data set for comparison.

The two remaining group IV spherules studied in detail were unusual in both appearance and composition —neither being consistent with known extraterrestrial, or terrestrial, spherules reported to date. Both plot close to the HED or Lunar lines on Fe-Mg-Mn systematics plots; however, these are also the regions over which terrestrial spherules plot. Both are also porous or vesicular and thus conceivably similar particles may not have been identified in Antarctic micrometeorite collections since they are likely mechanically weak and susceptible to weathering over time, especially if encased in ice or snow. If extraterrestrial in origin, these represent a new type of CS, one of which is transient in nature (with several examples occurring on one filter only) and the other is not unusual in that similar particles are identified on several filters.

The identification of unusual CSs should not be unexpected. The current classification scheme commonly adopted by micrometeorite researchers is that proposed by Genge et al. (2008), which divides samples according to the degree of atmospheric entry alteration (e.g., melted, partially melted, or unmelted) and their petrology (e.g., bulk chemistry, mineralogy, grain size). This classification scheme is by no means complete and, with further characterization of new micrometeorite collections, we should expect the current classification to need expanding and refining. Indeed, there are currently many micrometeorites from Antarctic collections with peculiarities that set them apart from the groups of the current classification scheme, but these are, at present, not numerous enough to establish their own category (for instance, the rare refractory mineral-bearing unmelted micrometeorites, e.g., Hoppe et al., 1995; Taylor et al., 2008).

Given that we are looking here at smaller particles than most previous studies, it is possible that the dominant dust production mechanisms responsible for these sizes may be different as a result of different inherent parent body properties. For example, the dust produced by a comet as a result of sublimation and loss of binding volatiles could have a very different size distribution to that of particles released by impact. Alternatively, the dust produced may depend on the inherent properties (e.g., strength) of the parent body and how these manifest in the size distribution of debris and dust produced by impacts. As a consequence, different parent bodies may be better represented in different dust size fractions. This idea has previously been invoked to explain why carbonaceous chondrite-like micrometeorites dominate smaller particle sizes (less than a few hundred micrometers in size), whilst increasing numbers of ordinary chondrite-like particles are identified amongst larger micrometeorites and meteorites (e.g., Suavet et al., 2010). Indeed, Flynn et al. (2009) showed that an order of magnitude more dust in the 30–300 μm size fraction was produced by impacts into carbonaceous chondrites compared with ordinary chondrites. This could also explain why other meteorite groups are under- or un-represented in micrometeorite samples: Achondritic micrometeorites, for example, account for only 0.5% of micrometeorites (Cordier et al., 2011; Gounelle et al., 2009; Taylor et al., 2007) whilst they account for ~8% of meteorite falls (Grady, 2000), and micrometeorites related to enstatite and R-type chondrites have yet been identified.

Further support to this idea of different size fractions representing different parent bodies comes from modeling: Briani et al., 2013 suggests that for a given entry velocity and angle, smaller particles suffer less heating and mass loss. Indeed, those few studies of smaller particles to date report high abundances of unmelted particles amongst this size range (e.g., Gounelle et al., 2005). If smaller particles can survive more oblique entry angles and higher velocities (either as melted or unmelted particles), it follows that perhaps this size range could contain samples from parent bodies not observed in those of larger particles. It is clear that further studies are needed to increase the data set of these smaller particles, from this and other collections.

We note here that perhaps more relevant samples for comparison against the group IV spherules in this study are the silicate spherules returned in stratospheric collections which are typically less than ~20 μm in size (e.g., Brownlee et al., 1982; MacKinnon et al., 1982). These particles were identified by Brownlee et al. (1982) as ablation spherules and thus not true micrometeorites. However, MacKinnon et al. (1982) argued that their compositions do not show typical chondritic abundances (as with our spherules) and thus they may, in fact, represent another type of particle worthy of further study. Clearly, high-precision analyses and comparisons of smaller (<50 μm) micrometeorites, including spherules from both surface and stratospheric collections, are needed and have the potential to make an extremely valuable contribution to our inventory of extraterrestrial samples available in the laboratory.

Identification of Terrestrial versus Extraterrestrial Particles

What is clear from this study is that to aid us in future assignment of extraterrestrial and terrestrial origins to particles, particularly those of unusual and unique types, further work to characterize the variety of terrestrial spherules, as well as extraterrestrial spherules, would be beneficial.

A crucial task in any micrometeorite collection study is to validate the identity of particles. Misidentification of terrestrial particles as micrometeorites causes significant bias in measurements of flux, and in the understanding of mineralogical and compositional diversity of extraterrestrial materials accreted to the Earth. A fundamental assumption made in particle identification is that modern day collections, such as Kwajalein, should be broadly similar in their range of extraterrestrial materials to those collected from Antarctica and deep-sea sediments, which sample extended periods of the micrometeorite flux. Supporting this assumption are observations of the cosmic spherules collected on rooftops, which exhibit similar types to Antarctic collections, and only minor differences in their relative abundances (Genge et al., 2016; Suttle et al., 2021). The occurrence of unique particle types, with atypical mineralogies, however, cannot be discounted in short-period collections since they can be biased by a single extraterrestrial source. Timed interplanetary dust particle collections, thought to sample Grigg-Skjellerup, for example, feature particles containing amphiboles (Busemann et al., 2009), which have yet to be identified amongst micrometeorites. However, despite their unique mineralogy, such particles still share the chondritic composition of primitive extraterrestrial materials. Unique non-chondritic materials could be identified as extraterrestrial through isotopic analyses (e.g., oxygen isotopic analyses; Folco & Cordier, 2015; Goderis et al., 2020; van Ginneken et al., 2017); however, the large number of different particles collected precludes the use of these techniques here. To overcome this, we can instead seek to identify potential terrestrial sources by studying available literature and assigning terrestrial origins to those particles that have mineralogical and/or compositional similarities to them. The potential sources of each group of recovered particles deemed terrestrial in origin are, therefore, now discussed separately below. We note that it is by no means complete, as a result of data lacking for terrestrial particles due to an absence of need. However, with the increased popularity of non-Antarctic micrometeorite collections, understanding potential terrestrial contaminants is now, more than ever, fundamental to the study and identification of such extraterrestrial materials.

Group I Sources

Group I spherules are those identified as terrestrial in origin, having compositions that are not consistent with any known CSs. Metallic Fe-rich group I spherules are likely anthropogenic, being readily produced by welding, either as weld spatter (droplets produced from disturbed molten metal) or fume particles (particles condensed from vapor created by intensely heated metal; Jenkins & Eagar, 2005). Both types of particle exhibit a wide variation in chemistry based on the metals being welded and, if using an electric arc as the energy source, the electrode and its coating (Kirichenko et al., 2018; Langway & Marvin, 1965). The use of grind wheels and high-speed drills provide additional mechanisms for the formation of metallic Fe-rich spherules (Larsen, 2016). In addition, Fe-rich spherules can be produced by combustion—so-called fly ash ferrospheres (e.g., Sokol et al., 2002; Valentim et al., 2016).

The Al-oxide spherules identified likely originate from rocket exhaust; Kwajalein Atoll is part of the Ronald Reagan Ballistic Missile Defense Test Site, and as such, the launch site for missile tests, anti-ballistic missile interception tests, meteorological sounding rockets, and Pegasus XL rockets. Al-oxide spherules are a common by-product of solid rocket fuel combustion produced when aluminum powder, used as a fuel additive in solid-fuel boosters, undergoes melting and oxidation. Such spherules have previously been identified in stratospheric particle collections, with sizes ranging from a few to 15 μm in diameter (e.g., Brownlee et al., 1976; Clanton & Gooding, 1985).

The Ti-oxide spherules are also likely anthropogenic. It is possible that they represent products of ablation of re-entering orbital debris; Fe- and Ti-rich spherules measuring a few to 15 μm in diameter have previously been observed in stratospheric samples and identified as such (Clanton & Gooding, 1985). Alternatively, Ti-rich spherules have also been identified in cork powder fly ash (referred to as titanspheres in Guimarães et al., 2020) with several examples containing Ti-oxide exhibiting dendritic growth identical in appearance to that of Fe-oxide dendrites commonly observed on cosmic spherules (thus highlighting the need to combine imaging and chemical analyses when verifying a cosmic origin). It is noted that such Ti-rich spherules have not yet been identified in the small size fractions (<50 μm) of Antarctic collections analyzed, yet for such origins they would be expected here also. This may, however, be a result of small numbers of the spherules in this size fraction being studied in detail to date.

The Fe-Ce-La-rich spherule (Figure 5l) is also an anthropogenic particle, derived from cigarette smoking. Ce and La are both components of mischmetal, which is

alloyed with iron to produce ferrocerium for use in artificial (lighter) flints (Paul et al., 2017). When struck, these flints create sparks and produce spherules ranging from ~1 to ~50 μm in diameter. This is not the first time that such rare earth element-rich particles have been identified in the search for extraterrestrial materials: Eight rare earth-rich spherules ranging from 30 to 50 μm in diameter were identified in samples of the meteorites Zagami and Murchison (Vieira et al., 1984a, 1984b). Although initially purported to be extraterrestrial in origin themselves, it was soon realized that they were surface contamination originating from handling by an individual who had recently used a lighter (Vieira et al., 1985).

Ca-rich particles identified as group I spherules are likely simply rounded naturally occurring rocky particles; however, two examples appear to resemble an iberulite (Figure 5e) and an ooid (Figure 5f). Iberulites are sedimentary spheroidal grains produced in the atmosphere (troposphere) by complex aerosol–water–gas interactions and ultimately the coalescence of smaller particles (Díaz-Hernández & Párraga, 2008). They are composed of a complex mixture of silicates, carbonates, sulfates, halides, oxides, and phosphate-vanadates and often incorporate biological remains (e.g., plants, silica shells, plankton). Iberuilites are typically 60–90 μm in diameter but smaller examples are observed. The particle in Figure 5f measures ~62 μm in diameter and is composed of a mixture of mineral grains consistent with being an iberulite. To date, iberulites have only been identified in modern passive collections of atmospheric dust from the Iberian Peninsula, where the specific atmospheric conditions combined with particulate supply from the Sahara desert are available, although it has been speculated that other iberulite-forming regions with the necessary conditions and materials may exist elsewhere (Díaz-Hernández & Snchez-Navas, 2016). The identification of an iberulite in our Kwajalein collections suggests either: that we have found another iberulite formation area, that there exists another mechanism for forming iberulite-like particles, or that we have demonstrated that global transportation of iberulites is possible. Ooids are another type of sedimentary spheroidal grain, which are composed of concentric layers of aragonite or aragonite and calcite accreted around a nucleus particle (e.g., a bioclast, peloid, siliciclastic grain, or lithoclast). Current models suggest that they form in marine or lacustrine environments through chemical precipitation which may, or may not, be induced or influenced by microbial activities (Diaz & Eberli, 2018). The particle in Figure 5f appears to have been broken in half, revealing it to be composed of a central nucleus surrounded by two layers. EDX data exhibit peaks for C, O, and Ca, suggesting a composition consistent with aragonite or calcite as observed for ooids. Such a particle formed in a marine environment could feasibly be lofted into the atmosphere by waterspouts, which are common in tropical climates.

A possible source for the remaining group I spherules (the Ca-P-rich, Cu-Cl-rich) could not be identified. For the Ca-P-rich spherules, which are nearly all identified on Filter 10, the idea that changes in weather conditions during the collection period could have driven the sudden influx of these particles was investigated. Weather station measurements of wind speed and direction taken over the collection periods, however, do not significantly deviate from average during the collection timeframe of Filter 10 (when the high influx of Ca-P-rich particles was noted); therefore, the source remains unknown.

Group II Sources

Group II Fe-rich spherules can exhibit chemistry and morphology consistent with I-type CSs. Fe-rich spherules are, however, known to be produced by a range of human activities as detailed for group I spherules above (e.g., combustion, welding, etc.). In particular, iron-rich fly ash ferrospherules are often dominated by magnetite that can be massive, dendritic, or finely crystalline (e.g., Sokol et al., 2002; Valentim et al., 2016) and thus closely resemble I-type CSs.

Group III Sources

Group III spherules are likely fly ash or volcanic in origin. Fly ash is the air-carried by-product of coal-fired power stations and consists of fine particles ranging from sub-micron to over 200 μm in diameter that are predominantly spherical in shape (Xu & Shi, 2018). Estimates for the amount of fly ash produced by coal-burning power plants range from over 350 million tons to approximately 750 million tons per year (e.g., Dwivedi & Jain, 2014; Yao et al., 2015). Power plants often use electrostatic precipitators and fabric filters to remove fly ash from plumes leaving the plant stacks and, when used correctly, can efficiently capture more than 99% of these particles (e.g., Goodarzi, 2006; Lind et al., 2003). However, malfunctions and operation errors can lead to much larger proportions of fly ash leaving the stack and entering the atmosphere (Blaha et al., 2008). These contributions, combined with contributions from those plants that do not use filtering systems at all, mean that fly ash is a common type of terrestrially derived spherule. Although Kwajalein is located >1000 miles from the nearest continent, and power here and on neighboring islands is provided by diesel generators, long-range transportation of fly ash has previously been demonstrated by its identification in samples from remote locations (e.g., Antarctic lake sediments; Rose et al., 2012) and thus it is likely to be present in the Kwajalein collections. Fly ash spherules can

have highly variable compositions dependent largely on the composition of the feed coal, or more specifically, the mineral matter within the coal (Ward & French, 2006) but they are predominantly silicates, and most commonly composed of silicon dioxide, aluminosilicate, and calcium aluminosilicate glasses (e.g., Aughenbaugh et al., 2016) consistent with our group III spherules. They can be solid spherules, referred to as microspheres, or hollow, referred to as cenospheres (Zyrkowski et al., 2016). Those hollow spheres that encase smaller spheres or mineral fragments within their void are referred to as plerospheres (e.g., Goodarzi & Sanei, 2008). Those composed of more than 70 wt% SiO_2 + Al_2O_3 + Fe_2O_3 and low in CaO (<12 wt %) are defined as class F fly ash and are derived from burning bituminous and antracitic coals, while those with between 50 and 70 wt% SiO_2 + Al_2O_3 + Fe_2O_3 and high in CaO (up to 40 wt%) are defined as class C fly ash and derived from burning sub-bituminous and lignite coals (Ahmaruzzaman, 2010). All fly ashes also commonly contain trace elements including Cr, Pb, Ni, Ba, Sr, V, and Zn (Yao et al., 2015). Available literature suggests that fly ash exhibits Mg-to-Si At% ratios no greater than 0.23, consistent with our earlier definition of group III (see Figure 7).

Glassy silicate spherules produced by volcanic activity are often referred to as Pele's tears or volcanic microspherules and are a component of volcanic ash produced predominantly by low-viscosity basaltic lava eruptions (e.g., Heiken, 1972; Lefèvre et al., 1986; Meeker & Hinkley, 1993; Mourne et al., 2007). They are generated when expanding gases within the lava coalesce and erupt at the surface, throwing out sprays of droplets in lava fountains—only rarely are they produced by medium to high-viscosity magmas (rhyolitic, dacitic, andesitic), with these being more likely to produce ash particles that are angular fragments (Heiken, 1972). Despite there being no active volcanoes locally within the Marshall Islands, volcanoes can eject huge volumes of ash high into the atmosphere, where it can circulate around the globe and ultimately settle far from its source (e.g., Ram & Gayley, 1991). As a very rough indication, assuming settling velocities ranging from approximately 0.003 to 0.2 m s^{-1} (applicable for particles 5–60 μm, ignoring effects of the atmospheric density profile and precipitation; Újvári et al., 2016), volcanic particles that reach stratospheric altitudes settle on the order of days to weeks; therefore, relevant eruptions to this collection are limited to those in 2011 and 2012. Indeed, in 2011, there were 75 confirmed volcanic eruptions, with six having a Volcanic Explosivity Index (VEI) value of 3 or more (generating substantial volumes of ash in plumes reaching >3 km) and in 2012, there were 80 volcanic eruptions, with four having a VEI value of 3 or more (https://volcano.si.edu/). It is, therefore, possible that volcanic microspherules are present in the Kwajalein collection. Volcanic microspherules are typically a few microns to several hundred microns in diameter (Mourne et al., 2007) and exhibit a range of surface textures from smooth to granular, and can be punctuated with vesicles or crystallites, cracked or coated in microparticles (e.g., Lefèvre et al., 1986; Meeker & Hinkley, 1993). Despite originating from basaltic lavas, volcanic microspherules also exhibit a wide range of chemical compositions. For example, one sampling from Etna's plume in 1998 containing spherules with SiO_2 ranging from 47 to 90 wt % and large variations in FeO (2 to 25 wt%), CaO (0 to 14 wt%), and Al_2O_3 (2 to 16 wt%) content (Spadaro et al., 2002). Furthermore, individual spherules can exhibit similar degrees of chemical zoning, with silica-enriched exteriors (Mourne et al., 2007). These variations in composition (both between spherules and within individual spherules) are believed to result from leaching that occurs in the volcanic plume, removing cations and leaving the particle enriched in silica (Spadaro et al., 2002). Based on the available literature cited above, the compositions reported for volcanic spherules are, therefore, variable but, as with silicate-dominated fly ash spherules, consistent with our definition of group III spherules (Figure 7) since they have Mg to Si At% ratios of <0.2 (indeed, in most cases $<<0.1$).

Related to volcanic activity, it has been shown that volcanic lightning occurring in eruptive columns and plumes can also produce spherules from volcanic ash (Genareau et al., 2015). Although no in-depth study of the composition of these lightning-induced volcanic spherules (LIVS) has yet been performed, it is possible that they too span a range of compositions: volcanic lightning can occur during any explosive eruption that generates ash, with no clear relations between the occurrence of lightning and magma composition identified (McNutt & Williams, 2010). However, available observational data suggest that, at most, 35% of volcanic eruptions are accompanied by lightning (McNutt & Williams, 2010). Furthermore, experiments suggest that conditions conducive to the production of LIVS are highly confined; Genareau et al., 2017 estimate that for the April 22nd–23rd 2015 eruption of Calbuco volcano where 1100 lightning strikes were observed, only on the order of 10^{-10} to 10^{-11}% of the entire eruptive column experiences conditions conducive to the formation of LIVS. Consequently, we do not anticipate finding LIVS in the Kwajalein collection.

Changes in Flux Over Time

The active nature of these collections, using a vacuum system to suck particles from the surrounding

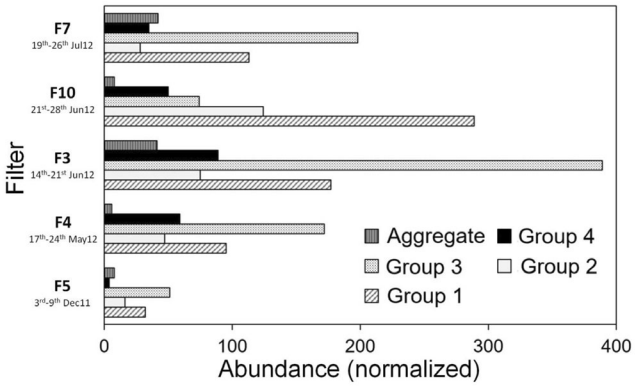

Figure 13. Comparison of particle abundances for each group on each filter. The abundance values plotted are those in brackets from Table 1 that have been calculated by normalizing to the maximum volume of air sampled by any filter (4739 m^3 by filter 4) and the total extent of the condensed area (~1018 mm^3).

air, means that although we have measured the size distribution of spherules in this collection (Figure 8), we cannot compare this against those derived from other collection methods. Close to the sampler, we can imagine that both small and large particles may feel the suction of the vacuum system and be pulled from their downward settling trajectory onto the filter. However, as the distance increases, the maximum particle size that will be sucked onto the filter decreases, such that the collection is biased toward smaller particles which may be sampled from a greater distance (Alesbrook, 2019). This is consistent with our size distribution findings (Figure 8) which show all four spherule groups peak in abundance in the 5–10 μm size bin (with particles smaller than 5 μm being smaller than the filter perforations and therefore lost to the vacuum system during collection/washing). The weekly changing of filters, however, enables us to investigate whether variations in particle abundances are observed over time in these collections and, if they are, to attempt to explain these variations with knowledge of local or recent events or conditions.

The number of spherules from each group that were identified on the filters is given in Table 1. The total volume of air that was sampled varied for each filter, most likely due to weather conditions (e.g., precipitation, wind strength, etc.) which would influence the degree/rate at which filter pores become blocked. Indeed, the dry season in the Marshall Islands occurs between December and April and its rainy season occurs between April and December, with greatest rainfall between July and October—in general, our filters exhibit a decreasing total volume of air sampled as collections move through June to the final filter collected at the end of July, when rains are heaviest. Furthermore, as stated in the methods section, although it was initially intended that image maps (produced to locate all possible spherules) be taken over one quadrant of the concentrated area of each filter, limited and varied instrument time available for individual maps meant they varied in size and thus the total area that was surveyed also ultimately varied for each filter. Consequently, to enable comparisons between abundances of each group of spherules on each filter, the values in brackets in Table 1 have been normalized by the ratio of the volume of air sampled to the maximum volume of air sampled by any filter (4379 m^3 by filter 4) and by the ratio of the area surveyed to the total extent of the condensed area (~1018 mm^3). These normalized values are compared in Figure 13. We note here that this assumes the distribution of particle types is homogenous across the entire condensed area—this is unlikely but provides an initial indication of variability across filters which must be confirmed by future studies of complete filters.

When the normalized values are compared for each filter, we see that those collected during the rainy season (Filters 4, 3, 10, and 7) exhibit total spherule numbers that are considerably higher (>3 times higher) than the filter collected during the dry season (Filter 5). This trend is not only observed for spherules, but for all particles, with the condensed stubs for the rainy season filters (Figure 4b–e) appearing more heavily populated with particles than the dry season filter (Figure 4a). This would suggest that particle abundances are heavily affected by the weather, with higher precipitation perhaps resulting in more efficient vertical transport of small particles (e.g., within water droplets). Additional filters from the dry season would need to be investigated to confirm this trend.

Comparing the normalized values for each group also reveals that there are variations observed for the different spherule types over time. Group I and II spherules appear to peak in abundance on Filter 10 while group III and IV spherules peak in abundance on Filter 3. For group I, much of the observed peak on Filter 10 is attributed to a sudden rise in the Ca-rich and Ca-P-rich particles whose origin is unknown, although the combined abundances of group I Al-oxide, Ti-oxide, and Fe-rich spherules also peak on this filter (2–7 times the abundance exhibited on the other filters). Assuming some local human activity was responsible for this peak in abundance, we considered known activities around this time and discovered that a Pegasus XL rocket carrying NASA's Nuclear Spectroscopic Telescope Array (NuSTAR) was launched from Kwajalein on 13th June 2012 (https://www.nustar.caltech.edu/page/launch), 8 days prior to the onset of collection by Filter 10. Since Filter 3, which began collecting 1 day after the launch, did not display a significant increase in abundance, this

implies a delay between launch and arrival at the filter of more than a week. If these are indeed linked to this rocket launch then this suggests the ground-based atmospheric collection method utilized in this project could potentially record short-term enhancement in all groups due to other local and/or recent events, for example, a local and/or recent volcanic eruption (group III) or a recent meteor shower (group IV). Although no volcanic eruption could be tied to the peak observed in group III particles on Filter 3 (this would likely be made difficult due to similarities with fly ash which is spread worldwide), the peak in group IV occurs approximately 2 weeks after the Earth's passage through the meteor stream associated with comet 73P/Schwassmann-Wachmann 3. The stream of this comet is of particular interest for two reasons. Firstly, it was highlighted as a comet that could potentially produce low-velocity Earth crossing debris streams on orbits with low inclination and low ellipticity, such that particles have a high potential to survive (not vaporize during) atmospheric entry (Messenger, 2002). Secondly, it was predicted that the debris stream would exhibit a significant enhancement in particle flux in 2012 (Messenger, 2011). As noted in the introduction, given the falling speeds calculated by Karsten (1968) for a 20-μm spherical grain of density 1 g cm^{-3} descending from an altitude of 80 km, the time taken to settle to the Earth's surface is estimated to be on the order of 26 days, meaning particles would not be expected at the surfaces until several days after Filter 3 finished collecting. Since there is great uncertainty in this settling time calculation (due to, e.g., variation in density, non-spherical morphology, assuming direct descent and therefore not accounting for the, likely considerable, influence of atmospheric circulation and weather, which vary over time and by location), it remains possible that the peak in abundance of group IV spherules on Filter 3 is linked to this meteor shower. However, given these particles would be cometary in origin, with favorable orbits for surviving atmospheric entry, we might expect them to be CP IDP-like rather than cosmic spherules. As these filters could not be surveyed for CP IDP-like particles due to the high volume of terrestrial dust present, we are unable to test this hypothesis here. We suggest that similar collections performed in locations of lower terrestrial background during times of such stream enhancements may be able to test the ability to collect and identify enhanced cosmic dust arrival at the Earth's surface.

Since the completion of this collection, several other ground-based atmospheric collections utilizing the same, or similar, vacuum systems to filter particles directly from the air have been performed both in the Antarctic at the British Antarctic Survey's clean air sector laboratory (CASLab) at the Halley VI Research Station (Alesbrook et al., 2017), at the Amundsen-Scott South Pole Station (Taylor et al., 2017, 2020), and on Hawai'i (Mauna Loa Observatory, Ishii et al., 2017). Preliminary studies of the Amundsen-Scott South Pole Station samples show promising results, with several IDP-like particles identified but, interestingly, no spherules (Taylor et al., 2020). This apparent lack of spherules may simply be the result of the different analysis procedures used, studying small, randomly selected locations on unprepared filters (not washed and particles are not condensed into a small region), such that any small number of spherules may be easily missed. Indeed, in the rare studies that have looked at particles from the smaller size fractions (<50 μm) removed from Antarctic snow, ice, and sediments, spherules are reported as being present (e.g., Gounelle et al., 2005; Noguchi et al., 2015), thus their entire absence from air-sampled collections in the Antarctic seems unlikely. However, it is possible that their apparent absence is the result of a real difference in small spherule flux between the two locations, with the flux being lower in the Antarctic (e.g., atmospheric circulation concentrating into one location whilst dispersing across others). Future analyses of these collections should seek to compare their spherule abundances (which will suffer the same collection biases detailed earlier and thus enable comparisons to be made) to investigate the possibility of location-dependent flux.

CONCLUSIONS

Our air sample collections from the mid-Pacific contained a range of dust particles, with filters containing far more particles than anticipated. This work, therefore, focused on the search for CSs, finding a range of terrestrial spherules that still dilute the sample set. We have identified 396 spherules and, using composition as an initial identifier, classified them into four groups. Groups I–III are likely terrestrial in origin while group IV was designated CS candidates and seven of these were studied in more detail. After examination, five of these candidates were deemed to be varieties of S-type CSs while the remaining two are unusual, and do not match either known terrestrial or extraterrestrial spherules. Having captured several CSs, we have demonstrated that ground-based atmospheric collection using high-volume air samplers is a viable method for the collection of micrometeorites. We have, however, also highlighted the need to further examine terrestrial sources of spherules for such non-Antarctic collections where terrestrial contamination is much greater. We have endeavored here to discuss potential sources based on current knowledge from literature.

Our analysis of particle abundances over time suggests that both terrestrial and extraterrestrial candidates appear

to fluctuate from filter to filter, highlighting the potential for such collections to preserve transient events, such as meteor showers. Since we have discovered, however, that only CSs could feasibly be studied in Kwajalein collections, in order to investigate the complete inventory of particles arriving at the Earth's surface, future collections using this method should also look to sampling from dryer, and cleaner, locations. Indeed, more complete results may be provided by similar collections that have been performed since the Kwajalein collection in the Antarctic at the British Antarctic Survey's clean air sector laboratory (CASLab) at the Halley VI Research Station (Alesbrook et al., 2017) and at the Amundsen-Scott South Pole Station (Taylor et al., 2017, 2020) as well as at the Mauna Loa Observatory in Hawai'i (Ishii et al., 2017).

Acknowledgments—The authors would like to thank R. Ogliore, C. Engrand, and J. Larsen for reviewing the manuscript and providing valuable comments and suggestions for improvement. We would also like to thank NASA for funding the collection on Kwajalein. We would also thank Dave Dearborn, Tory Jones, Blair Barnett, Steve Yakuma, and Tim Letendre for facilitating placement of the sampler of Kwajalein, help during the initial installation, and later replacing the motors of each of the samplers after the power surge in early 2012. We also thank Kirsten Hosek and Capelle Debrum for changing filters for the duration of the collection. The authors also thank Melissa Rodriguez, Ron Batien and Carla Gonzalez for their support during the project. PJW would like to thank a Marie Curie International Incoming Fellowship (298920—MICROMET-New Insights on micrometeorites) to study the Kwajalein filters. MvG would like to thank STFC.

Conflict of Interest Statement—The authors confirm there exist no conflicts of interest.

Editorial Handling—Dr. Maria Gritsevich

REFERENCES

Ahmaruzzaman, M. 2010. A Review on the Utilization of Fly Ash. *Progress in Energy and Combustion Science* 36: 327–363.

Akyuncu, V., Uysal, M., Tanyildizi, H., and Sumer, M. 2018. Modeling the Weight and Length Changes of the Concrete Exposed to Sulfate Using Artificial Neural Network. *Journal of Construction* 17: 337–353.

Alesbrook, L. S. 2019. *The Analysis of Two Unique Micrometeorite Collections, and the Effect of Atmospheric Entry on Extra-Terrestrial Particles*. Doctor of Philosophy (PhD) thesis, Canterbury, Kent, UK: University of Kent. (KAR id:84235). https://kar.kent.ac.uk/84235/.

Alesbrook, L. S., Wozniakiewicz, P. J., Jones, A. E., Price, M. C., Ishii, H. A., and Bradley, J. P. 2017. Atmospheric Collection of Extraterrestrial Dust at the Halley VI Research Station, Antarctica. *Lunar and Planetary Science Conference XLVIII*, abstract #1805, pp 2.

Aughenbaugh, K. L., Stutzman, P., and Juenger, M. C. G. 2016. Identifying Glass Compositions in Fly Ash. *Frontiers in Materials* 3: 1.

Bentz, D. P. 2014. Activation Energies of High-Volume Fly Ash Ternary Blends: Hydration and Setting. *Cement and Concrete Composites* 53: 214–223.

Bentz, D. P., and Ferraris, C. F. 2010. Rheology and Setting of High Volume Fly Ash Mixtures. *Cement and Concrete Composites* 32: 265–270.

Blaha, U., Sapkota, B., Appel, E., Stanjek, H., and Rösler, W. 2008. Micro-Scale Grain-Size Analysis and Magnetic Properties of Coal-Fired Power Plant Fly Ash and its Relevance for Environmental Magnetic Pollution Studies. *Atmospheric Environment* 42: 8359–70.

Bradley, J. P., Ishii, H. A., Wozniakiewicz, P., Noguchi, T., Engrand, C., and Brownlee, D. E. 2014. Impact of the Terrestrial Environment on the Compositions of GEMS. *Lunar and Planetary Science Conference XXXXV*, Abstract #1178, pp 2.

Brearley, A. J., and Jones, R. H. 1998. Chondritic Meteorites. In *Planetary Materials*, edited by J. J. Papike, vol. 36, C3-01-82. Washington D.C: The Mineralogical Society of America.

Briani, G., Pace, E., Shore, S. N., Pupillo, G., Passaro, A., and Aiello, S. 2013. Simulations of Micrometeoroid Interactions with the Earth Atmosphere. *Astronomy and Astrophysics* 552: A53.

Brownlee, D. E., Ferry, G. V., and Tomandl, D. 1976. Stratospheric Aluminium Oxide. *Science* 191: 1270–71.

Brownlee, D. E., Hodge, P. W., and Bucher, W. 1973. The Physical Nature of Interplanetary Dust as Inferred by Particles Collected at 35 km. In *Evolutionary and Physical Properties of Meteoroids, IAU Colloq*, edited by C. L. Hemenway, P. M. Millman, and A. F. Cook, vol. 13, 291–95. Washington D.C: NASA SP-319.

Brownlee, D. E., Olszewski, E., and Wheelock, M. 1982. A Working Taxonomy for Micrometeorites. *Lunar and Planetary Science Conference XIII*, pp 71-72.

Brownlee, D. E., Pilachowski, L. B., and Hodge, P. W. 1979. Meteorite Mining on the Ocean Floor. *Lunar and Planetary Science Conference X*, pp. 157–158.

Brownlee, D. E., Tomandl, D. A. and Olszewski E. 1977. Interplanetary dust; A New Source of Extraterrestrial Material for Laboratory Studies. Abstract of the Lunar and Planetary Science Conference VIII, pp. 145-147.

Busemann, H., Nguyen, A. N., Cody, G. D., Hoppe, P., Kilcoyne, A. L. D., Stroud, R. M., Zega, T. J., and Nittler, L. R. 2009. Ultra-Primitive Interplanetary Dust Particles from the Comet 26P/Grigg-Skjellerup Dust Stream Collection. *Earth and Planetary Science Letters* 288: 44–57.

Cano, E. J., Sharp, Z. D., and Shearer, C. K. 2020. Distinct Oxygen Isotope Compositions of the Earth and Moon. *Nature Geoscience* 13: 270–74.

Carrillo-Sánchez, J. D., Nesvorný, D., Pokorný, P., Janches, D., and Plane, J. M. C. 2016. Sources of Cosmic Dust in the Earth's Atmosphere. *Geophysical Research Letters* 43: 11979–86.

Clanton, U. S., and Gooding, J. L. 1985. Survey of Probably Micrometer-Sized Earth-Orbital Debris Fragments in the NASA/JSC Cosmic Dust Sample Collection. In Orbital Debris*: Proceedings of a Workshop Sponsored by NASA*

Lyndon B, edited by D. J. Kessler, and S.-Y. Su, 190–219. Houston, Texas: Johnson Space Center.

Cordier, C., Folco, L., and Taylor, S. 2011. Vestoid Cosmic Spherules from the South Pole Water Well and Transantarctic Mountains (Antarctica): A Major and Trace Element Study. *Geochimica et Cosmochimica Acta* 75: 1199–1215.

Davidson, J., Genge, M. J., Mills, A. A., Johnson, D. J., and Grady, M. M. 2007. Ancient cosmic dust from Triassic halite. *Lunar and Planetary Science Conference XXXVIII*, Abstract #1545, pp 2.

Diaz, D. R., and Eberli, G. P. 2018. Decoding the Mechanism of Formation in Marine Ooids: A Review. *Earth-Science Reviews* 190: 536–556.

Díaz-Hernández, J. L., and Párraga, J. 2008. The Nature and Tropospheric Formation of Iberulites: Pinkish Mineral Microspherulites. *Geochimica et Cosmochimica Acta* 72: 3883–3906.

Díaz-Hernández, J. L., and Snchez-Navas, A. 2016. Saharan Dust Outbreaks and Iberulite Episodes. *Journal of Geophysical Research: Atmospheres* 121: 7064–78.

Dredge, I., Parnell, J., Lindgren, P., and Bowden, S. 2010. Elevated Flux of Cosmic Spherules (Micrometeorites) in Ordovician Rocks of the Durness Group, NW Scotland. *Scottish Journal of Geology* 46: 7–16.

Duprat, J., Dobrică, E., Engrand, C., Aléon, J., Marrocchi, Y., Mostefaoui, S., Meibom, A., et al. 2010. Extreme Deuterium Excesses in Ultracarbonaceous Micrometeorites from Central Antarctic Snow. *Science* 328: 742–45.

Duprat, J., Engrand, C., Maurette, M., Kurat, G., Gounelle, M., and Hammer, C. 2007. Micrometeorites from Central Antarctic Snow: The CONCORDIA Collection. *Advances in Space Research* 39: 605–611.

Dwivedi, A., and Jain, M. K. 2014. Fly Ash – Waste Management and Overview: A Review. *Recent Research in Science and Technology* 6: 30–35.

Engrand, C., and Maurette, M. 1998. Carbonaceous Micrometeorites from Antarctica. *Meteoritics and Planetary Science* 33: 565–580.

Flynn, G. J., Durda, D. D., Minnick, M. A., and Strait, M. 2009. Production of Cosmic Dust by Hydrous and Anhydrous Asteroids: Implications for the Production of Interplanetary Dust Particles and Micrometeorites. *Lunar and Planetary Science Conference XXXX*, Abstract #1164.

Folco, L., and Cordier, C. 2015. Micrometeorites. In *Planetary Mineralogy*, edited by M. R. Lee, and H. Leroux, vol. 15. London, UK: The European Mineralogical Union and the Mineralogical Society of Great Britain & Ireland.

Fredriksson, K. 1956. Cosmic Spherules in Deep-Sea Sediments. *Nature* 177: 32–33.

Genareau, K., Gharghabi, P., Gafford, J., and Mazzola, M. 2017. The Elusive Evidence of Volcanic Lightning. *Scientific Reports* 7: 15508.

Genareau, K., Wardman, J. B., Wilson, T. M., McNutt, S. R., and Izbekov, P. 2015. Lightning-Induced Volcanic Spherules. *Geology* 43: 319–322.

Genge, M. J. 2008. Koronis Asteroid Dust within Antarctic Ice. *Geology* 36: 687–690.

Genge, M. J., Engrand, C., Gounelle, M., and Taylor, S. 2008. The Classification of Micrometeorites. *Meteoritics and Planetary Science* 43: 497–515.

Genge, M. J., Grady, M. M., and Hutchison, R. 1997. The Textures and Compositions of Fine-Grained Antarctic Micrometeorites—Implications for Comparisons with Meteorites. *Geochimica et Cosmochimica Acta* 61: 5149–62.

Genge, M. J., Larsen, J., Van Ginneken, M., and Suttle, M. D. 2017. An Urban Collection of Modern-Day Large Micrometeorites: Evidence for Variations in the Extraterrestrial Dust Flux through the Quarternary. *Geology* 46: 119–122.

Genge, M. J., Suttle, M., and van Ginneken, M. 2016. Olivine Settling in Cosmic Spherules during Atmospheric Deceleration: An Indicator of the Orbital Eccentricity of Interplanetary Dust. *Geophysical Research Letters* 43: 10646–53. https://doi.org/10.1002/2016GL070874.

Genge, M. J., van Ginneken, M., Suttle, M. D., and Harvey, R. P. 2018. Accumulation Mechanisms of Micrometeorites in an Ancient Supraglacial Moraine at Larkman Nunakak, Antarctica. *Meteoritics and Planetary Science* 53: 2051–66.

Goderis, S., Soens, B., Huber, M. S., McKibbin, S., van Ginneken, M., Van Maldeghem, F., Debaille, V., et al. 2020. Cosmic Spherules from Widerøefjellet, Sør Rondane Mountains (East Antarctica). *Geochimica et Cosmochimica Acta* 270: 112–143.

Goodarzi, F. 2006. Characteristics and Composition of Fly Ash from Canadian Coal-Fired Power Plants. *Fuel* 85: 1418–27.

Goodarzi, F., and Sanei, H. 2008. Plerosphere and its Role in Reduction of Emitted Fine Fly Ash Particles from Pulversized Coal-Fired Power Plants. *Fuel* 88: 382–86.

Goodrich, C. A., and Delaney, J. S. 2000. Fe/Mg-Fe/Mn Relations of Meteorites and Primary Heterogeneity of Primitive Achondirte Parent Bodies. *Geochimica et Cosmochimica Acta* 64: 149160.

Gounelle, M., Chaussidon, M., Morbidelli, A., Barrat, J.-A., Engrand, C., Zolensky, M. E., and McKeegan, K. A. 2009. A Unique Basaltic Micrometeorite Expands Inventory of Solar System Planetary Crusts. *Proceedings of the National Academy of Sciences* 106: 6904–9.

Gounelle, M., Engrand, C., Maurette, M., Kurat, G., McKeegan, K. D., and Brandstätter, F. 2005. Small Antarctic Micrometeorites: A Mineralogical and In Situ Oxygen Isotope Study. *Meteoritics and Planetary Science* 40: 917–932.

Grady, M. 2000. *Catalogue of Meteorites*. Cambridge, UK: Cambridge University Press. 696.

Guimarães, R., Guedes, A., and Valentim, B. 2020. Identification and Characterization of Ti-Spheres (Titanspheres) in Cork Powder Fly Ash. *Waste and Biomass Valorization* 11: 2905–23.

Heiken, G. 1972. Morphology and Petrology of Volcanic Ashes. *Geological Society of America Bulletin* 83: 1961–88.

Hoppe, P., Kurat, G., Walter, J., and Maurette, M. 1995. Trace elements and oxygen isotopes in a CAI-bearing micrometeorite from Antarctica. *Lunar and Planetary Science Conference XXVI*, p. 623.

Hutchison, R. 2004. *Meteorites A Petrologic, Chemical and Isotopic Synthesis*. New York: Cambridge University Press. 506.

Ishii, H. A., Wozniakiewicz, P. J., Bradley, J. P., Farley, K., and Martinsen, M. 2017. Extraterrestrial dust collection at Mauna Loa Observatory, Hawai'i. *Lunar and Planetary Science Conference XLVIII*, Abstract #1141, pp 2.

Jenkins, N. T., and Eagar, T. W. 2005. Fume Formation from Spatter Oxidation during Arc Welding. *Science and Technology of Welding and Joining* 10: 537–543.

Jonker, G., van Elsas, R., van der Lubbe, J. H. J. L., and van Westrenen, W. 2023. Improved Collection of Rooftop Micrometeorites through Optimized Extraction Methods:

The Budel Collection. *Meteoritics and Planetary Science* 58: 463–479.

Karsten, F. 1968. Falling Speed of Aerosol Particles. *Journal of Applied Meteorology* 7: 944–47.

Kearsley, A. T., Burchell, M. J., Price, M. C., Graham, G. A., Wozniakiewicz, P. J., Cole, M. J., Foster, N. J., and Teslich, N. 2009. Interpretation of Wild 2 Dust Fine Structure: Comparison of Stardust Aluminium Foil Craters to the Three Dimensional Shape of Experimental Impacts by Artificial Aggregate Particles and Meteorite Powders. *Meteoritics and Planetary Science* 44: 1489–1509.

Kirichenko, K. Y., Agoshkov, A. I., Drozd, V. A., Gridasov, A. V., Kholodov, A. S., Kobylyakov, S. P., Kosyanov, D. Y., et al. 2018. Characterization of Fume Particles Generated during Arc Welding with Various Covered Electrodes. *Scientific Reports* 8: 17169.

Kurat, G., Koeberl, C., Presper, T., Brandstätter, F., and Maurette, M. 1994. Petrology and Geochemistry of Antarctic Micrometeorites. *Geochimica et Cosmochimica Acta* 58: 3879–3904.

Langway, C. C., and Marvin, U. B. 1965. Some Characteristics of Black Spherules. *Annals of the New York Academy of Sciences* 119: 205–223.

Larsen, J. 2016. *In Search of Stardust, Micrometeorites and Other Spherules*. Arthouse DGB/Kunstbokforlaget den gyldene banan.

Law, D. W., Adam, A. A., Molyneaux, T. K., Patnaikuni, I., and Wardhono, A. 2015. Long Term Durability Properties of Calss F Fly Ash Geopolymer Concrete. *Materials and Structures* 48: 721–731.

Lefèvre, R., Gaudichet, A., and Billon-Galland, M. A. 1986. Silicate Microspherules Intercepted in the Plume of Etna Volcano. *Nature* 322: 817–820.

Lind, T., Hokkinen, J., Jokiniemi, J. K., Saarikoski, S., and Hillamo, R. 2003. Electrostatic Preciptator Collection Efficiency and Trace Element Emissions from co-Combustion of Biomass and Recovered Fuel Fluidized-Bed Combustion. *Environmental Science and Technology* 37: 2842–46.

Lopez-Flores, F. 1982. Flyash and Effects of Partial Cement Replacement by Flyash. In *Joint Highway Research Project JHRP-82-11*. West Lafayette, Indiana: School of Civil Engineering, Purdue University, 13 July 1982.

Love, S. G., and Brownlee, D. E. 1993. A Direct Measurement of the Terrestrial Mass Accretion Rate of Cosmic Dust. *Science* 262: 550–53.

Lugmair, G. W., and Shukolyukov, A. 1998. Early Solar System Timescales According to 53Mn-53Cr Systematics. *Geochimica et Cosmochimica Acta* 62: 2863–86.

MacKinnon, I. D. R., McKay, D. S., Nace, G., and Isaacs, A. M. 1982. Classification of the Johnson Space Center Stratospheric Dust Collection. In *Lunar and Planetary Science Conference XIII, Proceedings. Part 1. (A83-15326 04–91)*, A413–A421. Washington, DC: American Geophysical Union.

Maurette, M., Olinger, C., Christophe, M., Kurat, G., Pourchet, M., Brandstätter, F., and Bourot-Denise, M. 1991. A Collection of Diverse Micrometeorites Recovered from 100 Tonnes of Antarctic Blue Ice. *Nature* 351: 44–47.

McNutt, S. R., and Williams, E. R. 2010. Volcanic Lightning: Global Observations and Constraints on Source Mechanisms. *Bulletin of Volcanology* 72: 1153–67.

Meeker, G. P., and Hinkley, T. K. 1993. The Structure and Composition of Microspherules from Kilauea Volcano, Hawaii. *American Mineralogist* 78: 873–76.

Messenger, S. 2002. Opportunities for the Stratospheric Collection of Dust from Short-Period Comets. *Meteoritics and Planetary Science* 37: 1491–1505.

Messenger, S. 2011. Stratospheric collection of dust from comet 73P/Schwassmann-Wachmann 3. *Lunar and Planetary Science Conference XXXXII*, Abstract #2158, pp 2.

Messenger, S., Nakamura-Messenger, K., Keller, L. P., and Clemett, S. J. 2015. Pristine Stratospheric Collection of Interplanetary Dust on an Oil-Free Polyurethane Foam Substrate. *Meteoritics and Planetary Science* 50: 1468–85.

Mourne, S., Faure, F., Gauthier, P.-J., and Sims, K. W. W. 2007. Pele's Hairs and Tears: Natural Probe of Volcanic Plume. *Journal of Volcanology and Geothermal Research* 164: 244–253.

Nakamura, K., Nogushi, T., Ozono, Y., Osawa, T., and Nagao, K. 2005. Mineralogy of Ultracarbonaceous Large Micrometeorites. *Meteoritics and Planetary Science* 40: A110.

Nesvorný, D., Jenniskens, P., Levison, H. F., Bottke, W. F., Vokrouhlický, D., and Gounelle, M. 2010. Cometary Origin of the Zodiacal Cloud and Carbonaceous Micrometeorites. Implications for Hot Debris Disks. *The Astrophysical Journal* 713: 816–836.

Noguchi, T., Imae, N., Nakamura, T., Nozaki, W., Terada, K., Mori, T., Nakai, I., et al. 2000. A Consortium Study of Antarctic Micrometoeites Recovered from the Dome Fuji Station. *Antarctic Meteorite Research* 13: 270–284.

Noguchi, T., Ohashi, N., Tsujimoto, S., Mitsunari, T., Bradley, J. P., Nakamura, T., Toh, S., Stephan, T., Iwata, N., and Imae, N. 2015. Cometary Dust in Antarctic Ice and Snow: Past and Present Chondritic Porous Micrometeorites Preserved on the Earth's Surface. *Earth and Planetary Science Letters* 410: 1–11.

Paul, K. C., Silverstein, J., and Krekeler, M. P. S. 2017. New Insights into Rare Earth Element (REE) Particulate Generated by Cigarette Lighters: An Electron Microscopy and Materials Science Investigation of a Poorly Understood Indoor Air Pollutant and Constraints for Urban Geochemistry. *Environment and Earth Science* 76: 369.

Pettersson, H., and Fredriksson, K. 1958. Magnetic Spherules in Deep-Sea Deposits. *Pacific Science* 12: 71–81.

Ram, M., and Gayley, R. I. 1991. Long-Range Transport of Volcanic Ash to the Greenland Ice Sheet. *Nature* 349: 401–4.

Rietmeijer, F., Pfeffer, M., Chizmadia, L., Macy, B., Fischer, T., Zolensky, M., Warren, J., and Jenniskens, P. 2003. Leonid dust spheres captured during the 2002 storm? *Lunar and Planetary Science Conference XXXIV*, Abstract #1358, pp 2.

Rochette, P., Folco, L., Suavet, C., van Ginneken, M., Gattacceca, J., Perchiazzi, N., Braucher, R., and Harvey, R. P. 2008. Micrometeorites from the Transantarctic Mountains. *Proceedings of the National Academy of Sciences* 105: 18206–11.

Rojas, J., Duprat, J., Engrand, C., Dartois, E., Delauche, L., Godard, M., Gounelle, M., Carrillo-Sánchez, J. D., Pororný, P., and Plane, J. M. C. 2021. The Micrometeorite Flux at Dome C (Antarctica), Monitoring the Accretion of Extraterrestrial Dust on Earth. *Earth and Planetary Science Letters* 560: 116794.

Rose, N. L., Jones, V. J., Noon, P. E., Hodgson, D. A., Flower, R. J., and Appleby, P. G. 2012. Long-Range Transport of Pollutants to The Falkland Islands and Antarctica: Evidence from Lake Sediment Fly Ash Particle Records. *Environmental Science and Technology* 46: 9881–89.

Schramm, L. S., Brownlee, D. E., and Wheelock, M. M. 1989. Major Element Composition of Stratospheric Micrometeorites. *Meteoritics* 24: 99–112.

Siddique, R., and Khatib, J. M. 2010. Abrasion Resistance and Mechanical Properties of High-Volume Fly Ash Concrete. *Materials and Structures* 43: 709–718.

Sobolev, K., Flores, I., Bohler, J. D., Faheem, A., and Covi, A. 2014. Application of fly ash in ASHphalt Concrete: from Challenges to Opportunities. In proceedings of *World of Coal Ash Conference*, Cement and Concrete VI.

Sokol, E. V., Kalugin, V. M., Nigmatulina, E. N., Volkova, N. I., Frenkel, A. E., and Maksimova, N. V. 2002. Ferrospheres from Fly Ashes of Chelyabinsk Coals: Chemical Composition, Morphology and Formation Conditions. *Fuel* 81: 867–876.

Spadaro, F. R., Lefevre, R. A., and Ausset, P. 2002. Experimental Rapid Alteration of Basaltic Glass: Implications for the Origins of Atmospheric Particulates. *Geology* 30: 671–74.

Suavet, C., Alexandre, A., Franchi, I. A., Gattacceca, J., Sonzogni, C., Greenwood, R. C., Folco, L., and Rochette, P. 2010. Identification of the Parent Bodies of Micrometeorites with High-Precision Oxygen Isotope Ratios. *Earth and Planetary Science Letters* 293: 313–320.

Suavet, C., Cordier, C., Rochette, P., Folco, L., Gattacceca, J., Sonzogni, C., and Damphoffer, D. 2011. Orinary Chondrite-Related Giant (>800 μm) Cosmic Spherules from the Transantarctic Mountains, Antarctica. *Geochimica et Cosmochimica Acta* 75: 6200–6210.

Suavet, C., Rochette, P., Kars, M., Gattacceca, J., Folco, L., and Harvey, R. 2009. Statistical Properties of the Transantarctic Mountains (TAM) Micrometeorite Collection. *Polar Science* 3: 100–109.

Suttle, M. D., and Genge, M. J. 2017. Diagenetically Altered Fossil Micrometeorites Suggest Cosmic Dust Is Common in the Geological Record. *Earth and Planetary Science Letters* 476: 132–142.

Suttle, M. D., Hasse, T., and Hecht, L. 2021. Evaluating Urban Micrometeorites as a Research Resource – A Large Population Collected from a Single Rooftop. *Meteoritics and Planetary Science* 56: 1531–55.

Suzuki, A., Yamanoi, Y., Nakamura, T., and Nakashima, S. 2010. Micro-Spectroscopic Characterization of Organic and Hydrous Components in Weathered Antarctic Micrometeorites. *Earth, Planets and Space* 62: 33–46.

Taylor, S., Alexander, C. M. O'D., and Wengert, S. 2008. Rare micrometeorites from the South Pole, Antarctica. *Lunar and Planetary Science Conference XXXIX*, Abstract #1628, pp 2.

Taylor, S., Herzog, G. F., and Delaney, J. S. 2007. Crumbs from the Crust of Vesta: Achondritic Cosmic Spherules from the South Pole Water Well. *Meteoritics and Planetary Science* 42: 223–233.

Taylor, S., Lever, J. H., Alexander, C. M. O'D., Brownlee, D. E., Messenger, S., Nittler, L. R., Stroud, R. M., Wozniakiewicz, P. J., and Clemett, S. J. 2017. Sampling interplanetary dust particles from Antarctic air. *Lunar and Planetary Science Conference XLVIII*, Abstract #2024, pp 2.

Taylor, S., Lever, J. H., Burgess, K. D., Stroud, R. M., Brownlee, D. E., Nittler, L. R., Bardyn, A., et al. 2020. Sampling Interplanetary Dust from Antarctic Air. *Meteoritics and Planetary Science* 55: 1128–45.

Taylor, S., Lever, J. H., and Harvey, R. P. 1998. Accretion Rate of Cosmic Spherules Measured at the South Pole. *Nature* 392: 899–903.

Taylor, S., Lever, J. H., and Harvey, R. P. 2000. Numbers, Types and Compositions of an Unbiased Collection of Cosmic Spherules. *Meteoritics and Planetay Sciences* 35: 651–666.

Taylor, S., Matrajt, G., and Guan, Y. 2012. Fine-Grained Precursors Dominate the Micrometeorite Flux. *Meteoritics and Planetary Science* 47: 550–564.

Terada, K., Yada, T., Kojima, H., Noguchi, T., Nakamura, T., Murakami, T., Yano, H., et al. 2001. General Characterization of Antarctic Micrometeorites Collected by the 39th Japanese Antarctic Research Expedition: Consortium Studies of JARE AMMs (III). *Antarctic Meteorite Research* 14: 89–107.

Újvári, G., Kok, J. F., Varga, G., and Kovács, J. 2016. The Physics of Wind-Blown Loess: Implications for the Grain Size Proxy Interpretations in Quarternary Paleoclimate Studies. *Earth-Science Reviews* 154: 247–278.

Valentim, B., Shreya, N., Paul, B., Santos, G. C., Sant'Ovaia, H., Guedes, A., Ribeiro, J., et al. 2016. Characteristics of Ferrospheres in Fly Ashes Derived from Bokaro and Jharia (Jharkand, India) Coals. *International Journal of Coal Geology* 153: 52–74.

Van Ginneken, M., Folco, L., Cordier, C., and Rochette, P. 2012. Chondritic Micrometeorites from the Transantarctic Mountains. *Meteoritics and Planetary Science* 47: 228–247.

Van Ginneken, M., Gattacceca, J., Rochette, P., Sonzogni, C., Alexandre, A., Vidal, V., and Genge, M. J. 2017. The Parent Body Controls on Cosmic Spherule Texture: Evidence from Oxygen Isotopic Compositions of Large Micrometeorites. *Geochimica et Cosmochimica Acta* 212: 196–210.

Van Ginneken, M., Genge, M. J., Folco, L., and Harvey, R. P. 2016. The Weathering of Micrometeorites from the Transantarctic Mountains. *Geochimica et Cosmochimica Acta* 179: 1–31.

Van Ginneken, M., Wozniakiewicz, P. J., Brownlee, D. E., Debaille, V., Della, C. V., Delauche, L., Duprat, J., et al. 2024. Micrometeorite Collections: A Review and their Current Status. *Philosophical Transactions of the Royal Society A* 382: 20230195.

Vieira, V. W. A., Costa, T. V. V., Knudsen, J. M., and Jensen, G. B. 1984a. Small Spheres [30 μm – 50 μm] of $(CaRE)F_2$ and CaS in the Meteorites Zagami and Murchison. *Physica Scripta* 30: 384–85.

Vieira, V. W. A., Costa, T. V. V., Knudsen, J. M., and Jensen, G. B. 1984b. A Corrective Addendum on Previously Reported Small Spheres in the Meteorites Zagami and Murchison. *Physica Scripta* 30: 447–48.

Vieira, V. W. A., Costa, T. V. V., Knudsen, J. M., Jensen, G. B., Kemp, K., and Bastholm, N. H. 1985. Rare Earth Oxides and the Contamination Problem in Meteorite Research. *Physica Scripta* 31: 303–4.

Ward, C. R., and French, D. 2006. Determination of Glass Content and Estimation of Glass Composition in Fly Ash Using Quantitative X-Ray Diffractometry. *Fuel* 85: 2268–77.

Wozniakiewicz, P. J., Bradley, J. P., Price, M. C., Zolensky, M. E., Ishii, H. A., Brownlee, D. E., Dearborn, D., et al. 2014. Initial results from the Kwajalein micrometeorite collections. *Lunar and Planetary Science Conference XXXXV*, Abstract #1823, pp 2.

Wozniakiewicz, P. J., Ishii, H. A., Kearsley, A. T., Burchell, M. J., Bradley, J. P., Price, M. C., Teslich, N., Lee, M. R., and Cole, M. J. 2012. Stardust Impact Analogs: Resolving Pre- and Postimpact Mineralogy in Stardust Al Foils. *Meteoritics and Planetary Science* 47: 708–728.

Wozniakiewicz, P. J., Bradley, J. P., Zolensky, M. E., Brownlee, D. E., and Ishii, H. A. 2011. Kwajalein Atoll: A new collection site for micrometeorites. *74th Annual Meteoritical Society Meeting*, abstract #5206.

Wozniakiewicz, P. J., Bridges, J., Burchell, M. J., Carey, W., Della, C. J., Cort, V., Dignam, A., et al. 2021. A Cosmic Dust Detection Suite for the Deep Space Gateway. *Advances in Space Research* 68: 85–104.

Xu, G., and Shi, X. 2018. Characteristics and Applications of Fly Ash as a Sustainable Construction Material: A State-of-the-Art Review. *Resources, Conservation and Recycling* 136: 95–109.

Yao, Z. T., Ji, X. S., Sarker, P. K., Tang, J. H., Ge, L. Q., Xia, M. S., and Xi, Y. Q. 2015. A Comprehensive Review on the Applications of Coal Fly Ash. *Earth-Science Reviews* 141: 105–121.

Young, E. D., JKohl, I. E., Warren, P. H., Rubie, D. C., Jacobson, S. A., and Morbidelli, A. 2016. Oxygen Isotopic Evidence for Vigorous Mixing during the Moon-Forming Giant Impact. *Science* 351: 493–96.

Zhang, J., Dauphas, N., Davis, A. M., Leya, I., and Fedkin, A. 2012. The Proto-Earth as a Significant Source of Lunar Material. *Nature Geoscience* 5: 251–55.

Zolensky, M., Bland, P., Brown, P., and Halliday, I. 2006. Flux of Extraterrestrial Materials. In *Meteorites and the Early Solar System II*, edited by D. S. Lauretta, and H. Y. McSween, Jr., 869–888. Tuscon, Arizona: University of Arizona Press.

Zolensky, M. E., Pieters, C., Clark, B., and Papike, J. J. 2000. Small Is Beautiful : The Analysis of Nanogram-Sized Astromaterials. *Meteoritics and Planetary Science* 35: 9–29.

Zyrkowski, M., Costa, N. R., Santos, L. F., and Witkowski, K. 2016. Characterization of Fly-Ash Cenospheres from Coal-Fired Power Plant Unit. *Fuel* 174: 49–53.